

## Galaxy Groups at Intermediate Redshift

R. G. Carlberg<sup>1,2</sup>, H. K. C. Yee<sup>1,2</sup>, S. L. Morris<sup>1,3</sup>, H. Lin<sup>1,2,4,5</sup>,  
P. B. Hall<sup>1,2</sup>, D. R. Patton<sup>1,2</sup>, M. Sawicki<sup>1,2,7</sup>, and C. W. Shepherd<sup>1,2</sup>

### ABSTRACT

Galaxy groups likely to be virialized are identified within the CNOC2 intermediate redshift galaxy survey using an iterative method. The resulting groups have a median velocity dispersion of about  $200 \text{ km s}^{-1}$ . The virial mass-to-light ratios, using  $k$ -corrected and evolution-compensated luminosities, have medians in the range of  $150 - 250h \text{ M}_{\odot}/\text{L}_{\odot}$ . The number-velocity dispersion relation is in agreement with the low-mass extrapolation of the cluster normalized Press-Schechter function. The two-point group-group correlation function has  $r_0 = 6.8 \pm 0.3h^{-1} \text{ Mpc}$ , which is larger than the correlations of individual galaxies at the level predicted from  $n$ -body calibrated halo clustering. We conclude that the global statistics of groups are in approximate accord with dark matter halo predictions. The groups are stacked in velocity and position to create a sample large enough for measurement of a density and velocity dispersion profile. The resulting stacked group contains about 1000 members above a well defined background distribution. The stacked mean galaxy density profile falls nearly as a power law with  $r^{-2.5}$  and has no well-defined core. The projected velocity dispersion is examined for a variety of samples with different methods and found to be either flat or slowly rising outwards. The combination of a steeper-than-isothermal density profile and the outward rising velocity dispersion implies that the mass-to-light ratio of groups rises with radius. The  $M/L$  can be kept nearly constant if the galaxy orbits are nearly circular, although such strong tangential anisotropy is not supported by other evidence. The segregation of mass and light is not dependent on galaxy luminosity but is far more prominent in the red galaxies than the blue. The  $M/L$  gradient could arise from orbital “sloshing” of the galaxies in the group halos, dynamical friction acting on the galaxies

---

<sup>1</sup>Visiting Astronomer, Canada–France–Hawaii Telescope, which is operated by the National Research Council of Canada, le Centre National de Recherche Scientifique, and the University of Hawaii.

<sup>2</sup>Department of Astronomy, University of Toronto, Toronto ON, M5S 3H8 Canada

<sup>3</sup>Dominion Astrophysical Observatory, Herzberg Institute of Astrophysics, , National Research Council of Canada, 5071 West Saanich Road, Victoria, BC, V8X 4M6, Canada

<sup>4</sup>Steward Observatory, University of Arizona, Tucson, AZ, 85721

<sup>5</sup>Hubble Fellow

<sup>6</sup>Department of Physics & Astronomy, University of Victoria, Victoria, BC, V8W 3P6, Canada

<sup>7</sup>Mail Code 320-47, Caltech, Pasadena 91125, USA

in a background of “classical” collisionless dark matter, or, more speculatively, the dark matter may have a true core.

*Subject headings:* cosmology: large-scale structure, galaxies: evolution

## 1. Introduction

Small groups of galaxies are important cosmological indicators of the distribution and properties of the dark matter in the universe. They occupy the mass and velocity range between individual galactic halos and the large halos of rich galaxy clusters (Abell 1958; Burbidge & Burbidge 1960; Gott & Turner 1976; Hickson 1982; Ramella Geller & Huchra 1990; Nolthenius & White 1987). The RMS velocity dispersion of groups is only somewhat larger than that of individual galaxies, but groups have the advantage that visible galaxy tracers extend throughout the dark matter halo. At intermediate redshift, groups are suitable targets for X-ray observation and weak gravitational lensing studies which are complementary probes of their contents.. Consequently groups can be used to probe the properties of the dark matter on scales and at velocities much smaller than can be examined in galaxy clusters.

The theory of structure growth in the universe is based on the paradigm that the dark matter consists of collisionless particles that only interact via the gravitational force. Cold Dark Matter is a specific form of this hypothesis that has been subjected to intensive theoretical study. A particular strength is that the properties of virialized halos can be predicted from a given density perturbation spectrum to full nonlinearity via simulations and various analytic approximations. These predictions have been tested with varying degrees of success against the dark matter halos of individual galaxies and rich clusters, but are less examined on intermediate scales. The intermediate scales are interesting because they are at much higher phase space densities than massive galaxy clusters, yet their central dark matter densities are not overwhelmed and altered by the baryonic matter, as is the case in for most normal galaxies.

The CDM theory gives specific predictions of the statistical properties of the dark halo population and the mean internal properties of individual halos. The Press-Schechter theory (1974, hereafter PS) predicts the numbers of halos as a function of mass or velocity dispersion. At low redshift, suitably selected groups have a population volume density in accord with the cluster-normalized PS prediction (Moore Frenk & White 1993; Girardi & Giuricin 2000). A second global statistic is the clustering of dark matter halos which is predicted using analytic approximations which have been compared to n-body results (Mo & White 1996; Jing 1998). This biased “peaks” theory predicts a slow increase of clustering strength with halo mass. The internal density structure of the halos is found in simulations to have a power law cusp,  $r^{-1.0}$  to  $r^{-1.5}$  which asymptotically steepens to approximately  $r^{-3}$  beyond the virial radius (Dubinski & Carlberg 1991; Navarro, Frenk & White 1996; Moore et al. 1999a; Avila-Reese, Firmani, Klypin & Kravtsov 1999). The goals of this paper are to find a collection of

virialized groups and then to compare the predictions of the global statistics and internal structure of intermediate mass dark matter halos to the observationally derived properties.

The paper is organized as follows. The next section describes our approach to identifying groups in a redshift catalogue. Section 3 gives an overview of the Canadian Network for Observational Cosmology’s field galaxy redshift survey (CNOC2) and the virialized groups that we find. In §4 the number-velocity dispersion relation and the two-point correlation function are computed and compared to dark matter halo predictions. In §5 we “stack” the groups on their centers and measure the mean projected density distribution and projected velocity distribution. In §6 we model these as projections of simple 3D systems to derive the mean mass density profile and mass-to-light ratio as a function of radius which leads to the discovery that groups have a rising mass-to-light ratio. We examine the rising mass-to-light ratio for various galaxy sub-populations to search for systematic trends that might point to its physical origin. We conclude with a discussion of the possible implications of these results and a short set of empirical conclusions. We use  $H_0 = 100h \text{ km s}^{-1} \text{ Mpc}^{-1}$  throughout this paper and adopt  $\Omega_M = 0.2, \Omega_\Lambda = 0$  as our reference cosmological model. The distances and transverse lengths would be about 8% larger in an  $\Omega_M = 0.3, \Lambda = 0.7$  cosmology at the median redshift.

## 2. Finding Groups in Redshift Space

A group is defined here as a collection of three or more galaxies, above some minimum luminosity, that meets a set of positional requirements designed to minimize chance associations. One might seek, say, bound groups, such as the low overdensity Local Group, or, virialized groups, which are collapsed and hence quite dense. Virialized groups are a high density subset of bound groups and are the aggregates of interest in this paper. Unfortunately, in redshift space there is a fundamental degeneracy between position and line of sight velocity. Consequently, the precise galaxy membership of a group found in redshift space is always a statistical issue.

Most group search methods are based on the friends-of-friends (f-o-f) algorithm used by Huchra & Geller (1982). This is an important method that gives unique groups, independent of starting galaxy. The f-o-f algorithm can be tuned to yield groups of varying overdensity. The algorithm starts with any galaxy as the beginning of a trial group. All galaxies closer than some maximum distance (discussed below) are added to the group. Then, each of the new group members is in turn used as a center to search for its neighbors to add to the growing group, continuing until no more new neighbors are found. Then one proceeds to a previously un-examined galaxy to try to start a new group. This process continues until all galaxies have been examined for neighbors. Groups of one and two are then deleted from the catalogue.

The f-o-f algorithm has two parameters in redshift space: a maximum separation in projected radius,  $r_p^{max}$ , and either a maximum separation velocity,  $\Delta v^{max}$ , or co-moving redshift space distance difference,  $r_z^{max}$ , required to join the group. The  $\Delta v^{max}$  and  $r_z^{max}$  parameters are related

through  $\Delta v = H(z)r_z/(1+z)$ . We use  $\Delta v$  for kinematic measurements and  $r_z$  for group finding. The  $r_p^{max}$  and  $r_z^{max}$  parameters need to be mutually adjusted to take into account the mean volume density of the survey,  $n(z)$ , so as to produce an overdensity with respect to the field chosen on the basis of an experimental goal with an allowance for redshift space blurring. The resulting galaxy overdensity in the cylindrical redshift space search volume is,

$$\frac{\delta n}{n_0} \simeq \frac{1}{2\pi[r_p^{max}]^2 r_z^{max} n(z)}. \quad (1)$$

The  $r_z^{max}$  parameter needs to be chosen in relation to  $r_p^{max}$  with some care. One approach is to tune it to n-body simulation results (Nolthenius & White 1987). However, an ever-present issue is that the resulting group sizes and velocity dispersions tend to correlate with the  $r_p^{max}$  and  $r_z^{max}$  parameters.

Here we are interested exclusively in virialized groups, suggesting we devise a variant of the basic f-o-f algorithm which selects groups that appear to be sufficiently dense that they will quickly virialize. In configuration space virialization demands a mean interior density of approximately  $178\Omega^{0.45}\rho_c$  (Eke, Navarro & Frenk 1998), equivalent to nearly  $350\rho_0$  in a low density, flat cosmology. A conventional approximation is that such groups will be contained inside the radius  $r_{200}$  which can be estimated from the virial theorem as  $r_{200} = \sqrt{3}\sigma_1/[10H(z)]$ , where  $\sigma_1$  is the line-of-sight velocity dispersion and  $H(z)$  is the Hubble constant at the redshift of interest (Carlberg et al. 1996). For a given  $\sigma_1$  the virialized group members will be, on the average, contained within approximately  $1.5r_{200}$  if the mean density is falling like  $r^{-3}$ . This relation between velocity and projected separation immediately suggests a natural range for the parameters. The field pairwise velocity dispersion is approximately  $300 \text{ km s}^{-1}$  (Davis & Peebles 1983), equivalent to a single galaxy random velocity of about  $200 \text{ km s}^{-1}$ . This velocity dispersion is generated in groups which suggests that an average  $r_{200}$  will be about  $0.3h^{-1} \text{ Mpc}$  at  $z \sim 0.4$ .

The f-o-f algorithm provides a set of trial groups whose properties are fixed by the input link distance parameters such that many of them may not be virialized. Virialized groups have a minimum overdensity of about  $200\rho_c$ . Hence, for each trial group we estimate a velocity dispersion which is then used to calculate  $r_{200}$ . Galaxies beyond a distance to the group center of  $1.5r_{200}$  are discarded. The remaining galaxies are used to recalculate the velocity dispersion. This can be iterated until the group converges to a stable set. Some trial groups quickly drop to only one or two members and hence no longer qualify for group status. On the other hand, if we choose a very large starting value of  $r_p^{max}$  or  $\Delta v^{max}$  a few groups will percolate over very large structures. A minor complication is that we must identify a group center.

The details of our group finding algorithm follow. (1) Pick a cosmology for the analysis ( $H_0 = 100 \text{ km s}^{-1} \text{ Mpc}^{-1}$ ,  $\Omega_M = 0.2$ ,  $\Omega_\Lambda = 0$ ). (2) Set the sample's redshift and absolute luminosity limits (k-corrected and evolution-compensated at a mean rate of one magnitude per unit redshift) of  $M_R^{ke} = -18.5 \text{ mag}$ , no initial redshift limits) which defines a galaxy sample for all further operations. (3) Pick an  $r_p^{max}$  (our standard groups use  $0.25h^{-1} \text{ Mpc}$ ) and  $r_z^{max}$  ( $5 h^{-1} \text{ Mpc}$  for our standard groups). Center a cylinder of radius  $r_p^{max}$  and forward and backward extent of  $r_z^{max}$  on

each sample galaxy and count the number of sample galaxies. To create a background estimate we randomly draw points from an  $n(z)$  fitted to the full sample and count the number within the sample cylinder. If the search radii initially give less than three neighbors, then multiply smoothing lengths by 1.5 and repeat for this sample galaxy. At this stage a new subsample is defined requiring that the local overdensity relative to the smooth sample have some specified minimum value. In this paper we only impose the requirement that the local overdensity be positive. (4) Select the highest density ungrouped galaxy and begin to find a new group. (5) Standing on each new group member in turn, add to the group any galaxy in the minimum overdensity subsample that is closer than  $r_p^{max}$  and  $r_z^{max}$ . Repeat this step until no new galaxies are added. (6) This f-o-f group defines the starting group for the virialized group iteration. (7) For the trial virialized group, determine the geometric selection function weighted mean  $x$ ,  $y$ ,  $z$  and  $\sigma_1$ . Trim galaxies beyond, or add galaxies from the f-o-f list within,  $r_p = 1.5r_{200}$  and  $\Delta v = 3\sigma_1$ . Repeat step 7 four more times, requiring that the last two iterations have an identical result. (8) Drop single galaxies and pairs from the catalogue.

### 3. Groups in the CNOC2 Survey

The Canadian Network for Observational Cosmology Field Galaxy Redshift Survey (CNOC2) was undertaken primarily to study the dynamics of galaxy clustering at intermediate redshift. The survey methods and catalogues are fully described in Yee *et al.* (2000). The survey covers a total of about 1.5 square degrees in four patches spread around the sky for observing efficiency and to control cosmic variance. Galaxy redshifts are obtained over the redshift range 0 to 0.7, with the unbiased spectroscopic sample extending between redshifts 0.1 and 0.55. The catalogues contain approximately 6000 galaxy redshifts with an accuracy between 70 and 100 km s<sup>-1</sup>, along with UBVRI photometry. The groups are constructed from these catalogued galaxies. The luminosity and clustering evolution of the sample as a whole has been previously discussed (Lin et al. 1999; Carlberg et al 2000b).

The CNOC2 sample has  $m_R \leq 21.5$  mag and well defined spectroscopic completeness weights. The average redshift completeness is about 45%, with nearly 100% completeness 3 magnitudes above the limit and about 20% at the limit. Within our primary redshift range, 0.10 to 0.55, the redshift completeness to the flux limit is higher than for the sample as a whole. From our luminosity functions (Lin et al. 1999) we calculate the probability that we will successfully obtain a redshift as about 75% with the other 25% being for galaxies at redshifts out of our primary redshift range (Yee et al. 2000). Together these imply that about 60% of the galaxies above the flux limit in the redshift range 0.1 to 0.55 have measured redshifts. If a group contains 3 galaxies within the survey limits, then the probability from the cumulative binomial distribution that we will obtain 3 redshifts is  $(0.6)^3$  or 0.216. If the group contains 4 eligible galaxies then the probability we will obtain 3 or more redshifts rises to 0.47. The probabilities of obtaining 3 or more redshifts in groups of 5, 6, 7 and 8 eligible members are 0.68, 0.81, 0.90 and 0.95, respectively, assuming no complications

from geometric selection (Yee et al. 2000). Our average group contains 3.8 galaxies with redshifts. We conclude that our roughly one-in-two sampling allows us to detect about half of the three or more members groups that are present. This level of completeness has no bearing on most of our analysis so we normally do not attempt to compensate for this effect.

There is a small effect due to groups at the boundaries of the surveyed region. Examining a typical field we find that no more than 20% of the groups have any of their  $r_{200}$  area beyond the boundary and no more than half of that. Consequently approximately 10% of the group members are “missing”, which will have little effect on the velocity dispersions, and cause roughly a 10% diminution of the group masses, through the virial radius, and a similar effect on the total light. In the presence of much larger random fluctuations due to the small numbers in the groups this is not a major concern.

The only two parameters that turn out to have much of an impact on the groups are  $r_p^{max}$  and  $r_z^{max}$ . Our density requirement forces the “raw” groups to have a velocity dispersion strongly correlated with the search distance in the redshift direction,  $r_z^{max}$ . The effect of the iteration on the group velocity dispersion is shown in Figure 1. The initial velocity dispersion is calculated for the f-o-f groups and is hence very strongly correlated with the chosen  $r_z^{max}$ . The iteration to find virialized groups allows the  $\sigma_1$  values to relax to more appropriate values. However some less than ideal groups do persist which will lead us to continually consider alternate samples throughout this paper. Most of the groups converge to a stable membership in one or two iterations, with only 1-2% discarded due to failure to converge in four iterations.

Figure 2 shows the redshift distribution of the groups for four group catalogues with increasing  $r_z^{max}$ . Beyond redshift 0.45 the sample becomes incomplete as the flux limit of  $m_R = 21.5$  mag causes galaxies to slip below the sample absolute magnitude limit  $M_R^{ke} = -18.5$  mag. Both this figure and a detailed examination of the lists of groups shows that the sets of groups have a large overlap, independent of the search parameters. That is, this indirectly indicates that the set of group centers is relatively insensitive to the group finding procedure. In the next section we examine a variety of statistics to form a basis to select some group catalogues as best suited to various analyses.

#### 4. Global Properties of Groups and Halos

We will use three global properties of the groups to assess the degree of correspondence of various group catalogues to dark halos. These are the mass-to-light ratio distribution, the abundance as a function of velocity dispersion and the clustering properties. The virial mass to R band light ratio,  $M_{VT}/L_R$ , of groups is an indicator of the value of  $\Omega_M$ . The number density of dark matter halos as a function of their one-dimensional RMS velocity dispersion,  $n(\sigma_1)$ , is an important test of the CDM clustering spectrum but here is used as a guide to whether the number of high velocity dispersion groups is reasonable. The group-group auto-correlation as a function of mean separation,

$\xi_{hh}(r)$ , is a test of clustering theory. Together these indicators provide valuable information as to whether galaxy groups have approximately the properties expected on the basis that the galaxies are orbiting in a dark-matter dominated potential that is at least partially virialized.

Our statistical goals for group selection are to maximize the number of real groups and minimize the number of groups which contain redshift space interlopers. The derived group attributes come in three categories, with increasing sensitivity to the search parameters. First is the group centers,  $x, y$  and  $z$ ; second are the group extensions in  $r_p$ , and velocity, and third there are the specific galaxies in the groups. For all purposes the locations are key, whereas the extensions are secondary. The extensions do enter scaling relations, and the precise group membership is not relevant for averaged, background subtracted measurements.

#### 4.1. Virial Mass-to-Light Ratio

The ratio of the virial mass to the total luminosity,  $L_R^{k,e}$ , is a valuable indicator of the CDM mass density of the universe. It does not measure any component of the mass that clusters weakly. The virial mass-to-light ratio of groups has quite considerable scatter simply as a result of both small number statistics and orbital projection. On the basis of dynamical simulations Heisler, Tremaine & Bahcall (1985) found the dispersion in virial mass estimates as a result of these fluctuations is nearly a factor of two above and below the true mass, but this was comparable to other mass estimators. We calculate the virial mass,  $M_{VT}$ , using the galaxies in the groups with  $r_p \leq 1.5r_{200}$  and  $\Delta v \leq 3\sigma_1$ , following the CNOC methods (Carlberg et al. 1996). That is,

$$M_{VT} = \frac{3\pi}{2G} \sigma_1^2 R_h, \quad (2)$$

where the virial radius is evaluated for the galaxies identified as being group members. The circularly averaged harmonic radius is

$$R_h^{-1} = \left( \sum_i w_i \right)^{-2} \sum_{i<j} w_i w_j \frac{2}{\pi(r_i + r_j)} K(k_{ij}), \quad (3)$$

where  $k_{ij}^2 = 4r_i r_j / [(r_i + r_j)^2 + s^2]$  and  $K(k)$  is the complete elliptic integral of the first kind in Legendre's notation (Press *et al.* 1992). The softening,  $s = 2$  arcsecond, eliminates the divergence for galaxies at the same radii from the group center (Carlberg et al. 1996). The luminosity,  $L_R^{k,e}$ , is k-corrected, evolution compensated, and includes an extrapolation of the luminosity function to allow for galaxies below the redshift dependent absolute magnitude cutoff. The evolution is taken to be at a mean rate of one magnitude per unit redshift.

If group galaxies are drawn from a universal luminosity function and the ratio of dark mass to luminous mass is a constant then the median  $M_{VT}/L$  should be constant. The spread of the distribution of values can be used as an indicator of the statistical reliability of the group selection procedure. In Figure 3 we plot the median  $M_{VT}/L$  against the fractional difference between the

first and third quartile  $M_{VT}/L$  values. In the same system clusters have  $M_{VT}/L = 380 \pm 70 M_{\odot}/L_{\odot}$  (Carlberg et al. 1996), where we have removed the CNOC1 correction for the mean flattening of clusters. The median  $M_{VT}/L$  increases with both  $r_p^{max}$  and  $r_z^{max}$ . Groups selected with  $r_p^{max} = 0.5h^{-1}$  Mpc and large  $r_z^{max}$  have huge median  $M/L$  values and a large spread between first and third quartile values. Smaller  $r_z^{max}$  lead to an increase in the spread and decrease in the mean  $M_{VT}/L$ . The origin of this decrease in  $M_{VT}/L$  with size is at least partially a result of the internal  $M/L$  gradient within groups that we discuss below. Overall, the  $r_p^{max} = 0.25h^{-1}$  Mpc groups with  $r_z^{max} \leq 7h^{-1}$  Mpc have the desirable property that both the spread and the median of the distribution do not change too much with  $r_z^{max}$ .

The derived properties of the groups have very substantial uncertainties because of the small number of galaxies with velocities. The errors in the velocity dispersion and the resulting correlation with the derived virial mass-to-light ratios are illustrated in Figure 4 for the  $r_p^{max} = 0.25h^{-1}$  Mpc and  $r_z^{max} = 5h^{-1}$  Mpc groups. The large errors are the dominant source of the very strong correlation between the velocity dispersion and the derived  $M/L$ , as a consequence of  $M_{VT}$  as  $3G^{-1}\sigma_1^2 r_v$ , which accurately predicts the slope of the correlation visible in the figure. The inset diagram restricts the sample to groups with at least six members. In this case there is some support for the indication that the the mass-to-light ratio rises with velocity dispersion.

## 4.2. The Number Density-Velocity Dispersion Relation

The number of groups as a function of their line-of-sight RMS velocity dispersion is given in Figure 5 for a range of group search parameters. The median velocity dispersions for  $r_p^{max} = 0.25h^{-1}$  Mpc are 192, 229, 256 and 266 for  $r_z^{max}$  of 3, 5, 7, and  $10h^{-1}$  Mpc, respectively. Below  $100 \text{ km s}^{-1}$  is the regime of individual galaxies, which reduces the number of groups. A small effect is that the velocity precision of the survey is about  $100 \text{ km s}^{-1}$ , which artificially reduces the numbers of low velocity dispersion groups. At this stage we recall that large values of the search length in the redshift direction tends to include enough outlier galaxies that a few groups are promoted into the high  $\sigma_1$  tail of the distribution. Given that high velocity dispersion groups also tend to contain the most galaxies (for a constant  $M/L$ ), large groups are the easiest to find. Thus low membership groups with high velocity dispersions are likely to have erroneously large  $\sigma_1$  values.

The Press-Schechter (1974) theory works well to describe the abundance of halos in n-body experiments and a range of observational data, including clusters over a range of redshifts (Carlberg Morris Yee & Ellingson 1997) and low redshift groups (Girardi & Giuricin 2000). We can compare the Press-Schechter prediction for the number of groups to our observations. Because this requires absolute numbers we will use the redshift range of greatest completeness, roughly 0.2 to 0.45.

To calculate the expected density we follow the procedures outlined in Carlberg et al. (1997)



using  $\Omega_M = 0.2, \Omega_\Lambda = 0$  and  $\sigma_8 = 1.0$ . We calculate the mass-velocity dispersion relation as

$$M_{1.5} = 8.6 \times 10^8 \sigma_1^3 \text{ s}^3 \text{ km}^{-3} \text{ M}_\odot, \quad (4)$$

where  $\sigma_1$  is given in units of  $\text{km s}^{-1}$  and the mass is the nominal value inside a virialized  $1.5h^{-1}$  Mpc sphere, as is appropriate for rich clusters, to which we want to normalize these predictions. The equivalent top-hat radius that contains this mass at the mean density is

$$R_L \simeq 8.43 \Omega_z^{0.2p/(3-p)} \left[ \frac{M_{1.5}}{6.97 \times 10^{14} \Omega_M h^{-1} \text{ M}_\odot} \right]^{1/(3-p)} (1+z)^{-p/(3-p)} h^{-1} \text{ Mpc}, \quad (5)$$

where  $p \simeq 0.64$  is the rate of increase of mass with radius (White Efstathiou & Frenk 1993; Carlberg Morris Yee & Ellingson 1997) and  $\Omega_z$  is the value of  $\Omega_M$  at redshift  $z$ . We evaluate the Press-Schechter relation as

$$n(M(\sigma_1))dM = \frac{-3\delta_c(z)}{(2\pi r_L^2)^{3/2} \Delta} \frac{d \ln \Delta}{dM} \exp[-\delta_c^2(z)/2\Delta^2] dM, \quad (6)$$

where  $\delta_c(z) = 0.15(12\pi)^{2/3} \Omega^{0.0185}/D(z, \Omega)$ , (Navarro, Frenk & White 1996) and  $\Delta(r_L)$  is the top-hat fractional linear mass variance in spheres of radius  $r_L$  calculated using a fitted CDM spectrum (Efstathiou, Bond & White 1992). To determine the number density in bins of velocity dispersion we simply integrate over the relevant range of masses. Note that the normalization we have used automatically means that our group number densities will match on to the CNOC1 clusters (Carlberg Morris Yee & Ellingson 1997; Borgani, et al. 1999; Girardi & Giuricin 2000).

The Press-Schechter predictions of number density for a median redshift of 0.36 are displayed in Figure 5. The subsample is contained in a volume of  $1.8 \times 10^5 h^{-3} \text{ Mpc}^3$  (or about 50% more for a flat cosmology). Below  $100 \text{ km s}^{-1}$  the sample is missing many halos for two reasons. First, individual galaxy halos make up the majority of the halos in this regime. The velocity dispersion of an  $M_*$  elliptical is about equal to that of our median group (which in itself suggests an evolutionary connection). Second, because our velocity accuracy is about  $100 \text{ km s}^{-1}$  low velocity halos are scattered into the next higher bin. At this stage it we recall that our expected completeness rate for higher velocity dispersion groups is about 50% and even lower for those with velocity dispersions comparable to individual galaxies.

The Press-Schechter predictions are in reasonable agreement with the groups for  $r_z^{max} = 3h^{-1}$  Mpc and  $5h^{-1}$  Mpc, bearing in mind that the random errors are at least  $\sqrt{N}$ . Smaller values of  $r_z^{max}$  miss high  $\sigma_1$  groups, while larger values,  $r_z^{max} \geq 7h^{-1}$  Mpc, produce a few highly improbable groups with the velocity dispersions of rich clusters.

There are three reasons to select the  $r_p^{max} = 0.25h^{-1}$  Mpc and  $r_z^{max} = 5h^{-1}$  Mpc groups as the best suited to our analysis of virialized halos with velocity dispersions of approximately  $100\text{-}300 \text{ km s}^{-1}$ , although other group selection parameters give rise to samples that show a very similar set of  $x, y, z$  locations. The selected groups have a relatively low dispersion in their  $M/L$  values, their  $n(\sigma_1)$  distribution is close to the Press-Schechter prediction with few high velocity outliers,

and the dynamical analysis below finds that our chosen redshift distance inclusion length pulls in most of the group members so that the derived velocity dispersions are fairly stable against the addition of more outlying members with increasing cutoff velocity.

The locations on the sky of the “standard”  $r_z^{max} = 5h^{-1}$  Mpc and  $r_p^{max} = 0.25h^{-1}$  Mpc groups for one of the patches are shown as the points in Figure 6. The circles indicate the  $r_{200}$  radii. Note that some groups are quite compact with respect to this radius. The parameters of all of the standard groups are given in Table 1. The columns give the location with co-ordinates measured relative to the designated group centers (Yee et al. 2000),  $\sigma_1$  (from which  $r_{200}$  is calculated), the virial mass-to-light ratio, the number of group members with redshifts, and the mass. The random errors of the derived quantities, as estimated using the Jackknife technique, are very large for most of the groups, a straightforward consequence of the small numbers of members.

### 4.3. The Two-point Group-Group Correlation Function

A fundamental prediction of hierarchical dark matter clustering is that clustering, as measured by the two-point group correlation function  $\xi_{GG}(r)$ , should increase with the mass or velocity dispersion of the halo (Kaiser 1984; White et al. 1987). Here we measure both the redshift space correlation,  $\xi(s)$ , and the projected correlation function,  $w_p(r_p)$ , both of which provide an indication of the correlation length,  $r_0$ . The co-moving redshift space separation is,

$$s^2 = [r(\frac{1}{2}z_1 + \frac{1}{2}z_2)(\theta_1 - \theta_2)]^2 + [r(z_1) - r(z_2)]^2, \quad (7)$$

with  $r(z)$  being the co-moving distance at redshift  $z$ . At separations small compared to the pairwise-velocity converted to a distance,  $\sigma_{12}/H(z)$ ,  $\xi(s)$  ceases to increase with decreasing separation as the random velocities begin to dominate the redshift space separation. On larger scales  $\xi(s)$  is expected to be enhanced relative to  $\xi(r)$  as a result of the “compression effect” of systematic infall (Kaiser 1987).

The projected correlation function,  $w_p(r_p) = \int \xi[\sqrt{r_p^2 + r_z^2}] dr_z$ , has the advantage that the peculiar velocities have no effect on the result (Davis & Peebles 1983). We use the classical  $DD/DR - 1$  estimator (Peebles 1980) which is suitable in the strong correlation regime. The random distribution is derived from a fit to the observed  $n(z)$  distribution of the groups. Pairs are included for  $r_z$  up to  $30h^{-1}$  Mpc, co-moving. For a power law correlation function,  $\xi(r) = (r_0/r)^\gamma$ , the reduced projected correlation function,  $w_p/r_p$  is equal to  $A(\gamma)\xi(r)$ , where  $A(\gamma) = \Gamma(\frac{1}{2})\Gamma(\frac{1}{2}(\gamma - 1))/\Gamma(\frac{1}{2}\gamma)$ , a factor of 3.68 for  $\gamma = 1.8$  (Davis & Peebles 1983).

We evaluate the correlations using the same procedures and programs used in Carlberg et al. (2000) to measure the correlation of galaxies. Using the standard group sample ( $r_p^{max} = 0.25h^{-1}$  Mpc and  $r_z^{max} = 5h^{-1}$  Mpc) we evaluate  $\xi(s)$  and  $w_p(r_p)/r_p$  over the redshift range 0.15 to 0.55. We use as much redshift range as possible to boost the sample size. The resulting correlation functions are displayed in Figure 7. In the form plotted both functions are dimensionless

functions. Note that the upward offset of  $w_p(r_p)/r_p$  relative to  $\xi(s)$  is a natural result of the  $A(\gamma)$  factor. The error flags displayed in the figure are the square root of the number of galaxy pairs in each bin. Fitting the measured redshift space correlations to the function  $\xi(r) = (s_0/r)^{1.8}$ , gives  $s_0 = 6.8 \pm 0.3h^{-1}$  Mpc. The fit for the projected correlation function finds  $r_0 = 6.5 \pm 0.3h^{-1}$  Mpc. These errors are formal fitting errors and do not include an allowance for the patch-to-patch variance which likely dominates the random error.

The correlations measured for the CNOC2 galaxies over this redshift range in this cosmology have a mean of  $r_0 = 4.2 \pm 0.2h^{-1}$  Mpc where this error includes the patch-to-patch variance (Carlberg et al 2000b). The ratio of the correlation amplitude of our groups to that of the galaxies is  $2.2 \pm 0.4$ . At low redshift, Ramella, Geller & Huchra (1990) found  $s_0 \simeq 8h^{-1}$  Mpc for the CfA groups, which are somewhat lower mean internal density than ours. A similar result emerged for the combination of the CfA and SSRS2 groups (Girardi Boschin & da Costa 2000) which found that the group correlation amplitude was a factor of  $1.64 \pm 0.16$  stronger than that of galaxies, although the CfA groups alone appeared to have a smaller offset.

The biasing theory of Mo & White (1996) gives predictions of the expected ratio of correlation amplitudes. The characteristic velocity dispersion of normal galaxies is about  $100 \text{ km s}^{-1}$ , whereas our groups have a median velocity dispersion of about  $200 \text{ km s}^{-1}$ . From the CDM power spectrum (Efstathiou, Bond & White 1992) with a shape parameter of  $\Gamma = 0.2$ , we calculate the linear mass variances to be 3.3 and 2.4, for 1 and  $2h^{-1}$  Mpc top-hat perturbations, which are approximately the unperturbed mean radii of the perturbations associated with galaxies and groups, respectively. With  $\delta_c \simeq 1.68$  in the Mo & White model, we find that groups should be more strongly correlated by a factor of about 1.75 or 1.47 with the Jing (1998) n-body calibrated modification. Provided that the group velocity dispersion is about twice the galaxy velocity dispersion the results are not very sensitive to the velocity dispersions chosen. We conclude that the correlation amplitudes are consistent with the expected relation at about the 1.5 standard deviation level.

At this stage we have shown that our sample of groups is in good accord with three global statistics predicted on the basis of galaxies tracing cold dark matter halos. The next issue is to examine the relative internal distribution of the dark matter relative to the galaxies.

## 5. Mean Internal Structure of the Groups

N-body simulations now have sufficient length resolution that they can reliably predict the highly nonlinear realization of the collapse of halos and their resulting internal density profile. A fundamental prediction is that CDM halos have a central density cusp, roughly  $r^{-1.0}$  to  $r^{-1.5}$  (Dubinski & Carlberg 1991; Navarro, Frenk & White 1996; Moore et al. 1999a; Avila-Reese, Firmani, Klypin & Kravtsov 1999). At large radii the density begins to drop as approximately  $r^{-3}$ . The characteristic radius of the density profile can be calibrated in n-body experiments and derived from an approximate theory (Navarro, Frenk & White 1996). For the

massive dark matter halos of rich clusters the NFW density function,  $\rho(r) = Ar^{-1}(r + a)^{-2}$ , is entirely consistent with the derived mass distribution (Carlberg et al. 1997). The situation for galaxy mass halos is somewhat controversial, with constraining data coming from disk rotation curves in the presence of substantial amounts of baryonic mass and the modeling complication of partial pressure support relative to the circular velocity. However there is evidence that in small velocity dispersion halos CDM may allow central densities that exceed the observations (Moore et al. 1999a; Moore et al. 1999b).

A fundamental difference between a galaxy and a rich cluster of galaxies is that galaxies have a strongly rising mass-to-light ratios with increasing distance from the center whereas rich galaxy clusters have a nearly constant mass-to-light ratio over their virialized volume (Carlberg Yee & Ellingson 1997). Therefore a basic question is whether groups exhibit a rising mass-to-light ratio. Individual groups have too few galaxies to make such a measurement. Moreover groups come with a wide range of galaxy contents and have somewhat uncertain virialization because of their small numbers. Therefore we assemble a “stacked” mean group to boost the numbers to levels where we can make reliable measurements of the density and velocity dispersion profiles.

### 5.1. The Stacked Mean Group

Precisely how the mean group is built from the individual groups will have a significant impact on its properties. For instance, poorly determined centers will create a core in the projected profile, or, overlaying a small low velocity dispersion group with a large high velocity dispersion group will lead to a rising velocity dispersion with radius. The idea is simple: we stack galaxies in both  $r_p$  and  $\Delta v$  on the group centers keeping track of the expected number of background galaxies. All galaxies are used, with no distinction given to galaxies that were used to define the group center. The group centers are determined in the virial analysis as the geometric weighted mean of the locations of the iteratively selected group members. We have adopted geometric weights, which help to compensate for the objects without redshifts. The smoothing radius used to calculate our geometric weights is  $120''$  which is so large that there is little weight variation within these small groups, but weights do vary from group to group. That is, at the  $x, y, z$  location of each of the  $n_G$  groups in turn, we count the number of galaxies in the neighborhood at separations  $r_p/r_{200}$  and  $\Delta v/\sigma_1$ , to measure the stacked density distribution in redshift space of a group,  $n_{Gg}(r_p, \Delta v)$ . The stacked density distribution is related to the two-dimensional group-galaxy correlation function,  $\xi_{Gg}$  as,

$$n_{Gg}(r_p, \Delta v) = n_G n_g(z) \left[ \xi_{Gg} \left( \frac{R}{r_{200}}, \frac{\Delta v}{\sigma_1} \right) + 1 \right], \quad (8)$$

where  $n_g(z)$  is a smoothed fit to the redshift distribution locally converted to velocities in precisely the same way as the real galaxy pairs. This is the  $DD/DR-1$  method (Peebles 1980) of calculating a cross-correlation between groups and galaxies. The correlation function  $\xi_{Gg}$  is the fundamental

quantity of interest, since it has the background density removed. Both the surface density profile and the velocity dispersion profile are derived from  $\xi_{Gg}$ . Note that the total luminosity of the group uses the magnitude weights, which allows for the declining sampling rate towards the sample limit. Figure 6 builds the confidence that the selected centers are entirely sensible, although at this stage we cannot claim that this is an optimal procedure.

To assemble our “standard” mean group we will scale all the velocities to the  $\sigma_1$  measured for each group and the radii to the  $r_{200}$  derived from the velocity dispersion. Because there is a substantial uncertainty in  $\sigma_1$  for these small groups there is a concern that these scalings contain a large random element. At some level this is unavoidable. As the galaxies orbit in the groups they will have different velocities and positions with time which because of the little averaging available in small groups leads to considerable variation of their redshift space properties. Scaling the velocities and the radii avoids the pitfall of overlaying small, low velocity dispersion groups on the inside and large, high velocity dispersion groups on the outside, which would immediately lead to a rise of velocity dispersion with radius. The plot of the radial location of each galaxy that contributes to the mean group as a function of the source group’s velocity dispersion in Figure 8 does show one potential systematic problem: the higher velocity dispersion groups do not extend out to  $1.5r_{200}$ . This suggests that redshift space interlopers are an important source of noise leading to velocity dispersions that are too large for the size of the group. To address this issue we will be considering a number of alternate groups samples to check our results.

Although these groups have small numbers of members interlopers can be accurately removed statistically. We use the smoothed  $n_g(z)$  that we derive from the galaxy sample as a whole using the procedures of our clustering analysis (Carlberg et al 2000b). The random data are scaled in precisely the same way as the true data to determine whether or not they are in the cluster. To do the subtraction we need to bin the mean group in  $r_p$  and  $\Delta v$  bins. We select bins that are 0.2 dex in  $\log_{10}(r_p/r_{200})$  and 0.1 in the velocities scaled to  $\sigma_1$ . The binning is needed in our subsequent analysis anyway. We make velocity distance cuts at 3, 4 and 5 units as a check on the effect of residual interlopers and normally use the minimal noise 3 unit cut as our standard dataset.

Although we have statistically subtracted the background, the velocity dispersion estimate is very sensitive to the presence of field interlopers. In physical co-ordinates the densities of the groups are expected to be about  $100\rho_0$  near  $r_{200}$ , but this is reduced by a factor of roughly  $3\sigma_1/[H(z)r_{200}] \simeq 20$  at our  $\Delta v = 3\sigma_1$  cutoff. Consequently interlopers, which are distributed nearly uniformly in distance, generally cause erroneously large velocity dispersions. If there is a constant density normalization underestimate then the fraction of interlopers will increase with  $r_p$ , since the contrast between the group and the surrounding field declines with increasing  $r_p$ .

The probability of group interlopers can be estimated from the two-point correlation function. The probability that a galaxy with  $r_p \leq r_p^{max}$  and  $\Delta v < \Delta v^{max}$  is physically within  $r < r_p$  is discussed in Carlberg *et al.* (2000a). The conclusion is that slightly more than 50% of the galaxies within the required velocity separation are within the required radial separation,  $r$ . The other 50%

are clustered towards the group but most probably at roughly a correlation length. Other than small factors of order unity this redshift to real space ambiguity always exists. This means groups of size  $n$  may well be of size  $n - 1$ . The chances that they are of size  $n - 2$  drops precipitously. Of course as  $n$  rises the fraction of interlopers is falling. These correlated but unvirialized group galaxies cannot be avoided. Although they present a challenge for a particular group they are not a significant complication for most statistical analyses of the mean group, given the mean group density profile we derive below.

## 5.2. The Mean Density Profile

Summing the mean group over velocities gives the mean projected density profile displayed in Figure 9. The points are for cutoffs at 3, 4 and 5 velocity units, with the points declining slightly at small radii for increasing velocity cutoffs as a result of the normalization of the total integrated density to unity. The errors are evaluated from the patch-to-patch variance. There is little systematic change with increasing velocity cutoff. It is immediately clear that the projected density profile is very nearly a power law with only a weak break to a slightly shallower central profile. The mean projected slope of our virialized groups is approximately  $\Sigma_N \propto R^{-1.5}$ . The effect of restricting the sample to the  $\sigma_1 \leq 200 \text{ km s}^{-1}$  groups is shown in the inset to Figure 9. The density profile becomes somewhat steeper at large radii and there is a suggestion there is a break in the power law at small radii. The best fit parameters are  $a \simeq 0.7$  and  $b \simeq 2.5$ , although the core slope is not well defined.

We model the projected galaxy density distribution as the projection of the galaxy number density distribution,

$$\nu(r) = \frac{A}{4\pi r^a (r + c)^b}, \quad (9)$$

which is projected to a surface density using

$$\Sigma_N(R) = 2 \int_R^\infty \nu(r) \frac{r}{\sqrt{r^2 - R^2}} dr. \quad (10)$$

so that we minimize the variance in the  $\Sigma_N(R)$  plane. The resulting best fit is degenerate because the scale radius is always found to be very small. For the data displayed we find  $c = 0.061, 0.074$  and  $0.062$ , for cutoffs of 3, 4 and 5, respectively. The  $[a, b]$  pairs are  $[0.50, 2.05]$ ,  $[0.81, 1.71]$ , and  $[0.78, 1.71]$ , respectively. However, other fits with  $a + b = 2.55 \pm 0.05$  are equally acceptable given the small implied scale radius,  $c$ .

It is somewhat remarkable that using our mean group center we identify such a cusped density profile. The procedure is not guaranteed to have any galaxy at the center of the group, whereas we find that on the average the galaxy density declines quite steeply away from the center. This is quite different from the cluster situation where a similar average center gives a reduced central density (Carlberg Yee & Ellingson 1997). The NFW profile does not provide a good fit to this

distribution of galaxies, although it must be borne in mind that the NFW model describes the dark matter profile, not the galaxy distribution which can in principle be quite different. Our observed group profile is near a power law which is steeper in the center and shallower at large radii, than the NFW function or the steeper central cusps found by others (Moore et al. 1999a; Avila-Reese, Firmani, Klypin & Kravtsov 1999).

### 5.3. The Mean Velocity Dispersion Profile

The velocity dispersion profile allows the mass profile to be constrained. The projected velocity dispersion profile,  $\sigma_p(R)$ , for the  $r_z^{max} = 5h^{-1}$  Mpc groups is shown in Figure 10. It is crucial that the weak rise, or at least absence of a decline, in the projected velocity dispersion with radius be real, not an artifact of inadequate background subtraction. We display the results for several alternate values of  $r_z^{max}$  in Figure 11, and find that all give similar velocity dispersion profiles. Figure 11 also shows that setting  $r_z^{max}$  larger than the standard tends to increase the noise, while smaller values tend to leave out genuine group galaxies in the  $\sigma_1$  estimate so that larger velocity cutoffs quickly lead to higher  $\sigma_p(R)$ .

To help understand the distribution of possible outliers we present Figure 12, a gray scale of the  $r_p - \Delta v$  plane of the mean group profile, normalized to  $\xi_{Gg}(r_p, \Delta v)/\Sigma(r_p)$ , to remove the surface density variation. The plot shows that inside of about  $0.05r_{200}$  the statistics are too poor to give useful results. Beyond about  $2r_{200}$  there is no expectation that the galaxies are in virial equilibrium. The figure provides evidence that the slow rise in velocity dispersion across the virialized region is real and not a consequence of increasing interlopers with radius. Beyond about  $2r_{200}$  virialized motions are small and the width of the distribution increases rapidly. The slow rise of  $\sigma_p(R)$  is clearly rooted in the data, although a constant  $\sigma_p$  is not strongly excluded. It is well known that the pairwise velocity dispersion of galaxies has a similar weak rise with increasing separation; however that is expected on the basis of the two-point correlation function falling as  $r^{-1.8}$ , rather than the  $r^{-2.5}$  that we find here. A dynamical constraint from the Jeans equation is that in a scale free distribution,  $\sigma^2 \propto \rho(r)r^2$ . Therefore, the surprising outcome is the combination of the “steep”  $\Sigma(R)$  and “slowly-rising”  $\sigma_p(R)$ . Interlopers are always a concern but will tend to increase the outer values of both these functions, to leave the discrepancy in place.

To evaluate the significance of the radial trends we require reliable errors estimates. The errors in  $\Sigma(R)$  and  $\sigma_p(R)$  are robustly and empirically evaluated from the patch-to-patch variances in the quantities of interest. We find that the sensitivity to the velocity cutoff is relatively small, except that the errors increase in size. As a consequence we will use the 3 velocity unit cutoff as our standard. The velocity dispersion is calculated as the second moment of the binned projected velocity distribution function (pvdF). Figure 13 displays the average pvdF, normalized to the velocity dispersion in each radial bin. We note that the observed pvdF is much closer to Gaussian than to an exponential, although relative to the Gaussian the group mean pvdF appears to have a small excess at small and large velocities. This pvdF indicates that only mild anisotropy is allowed

(van der Marel et al. 2000), at least for simple distribution functions.

The projected velocity dispersion is easily modeled as the projection of a 3D velocity dispersion, where we adjust the radial velocity dispersion,  $\sigma_r(r)$ , and the velocity anisotropy,  $\beta(r)$ , to fit the data. The projection integral is,

$$\sigma_p^2(R)\Sigma_N(R) = \int_R^\infty \nu(r)\sigma_r^2 \left(1 - \beta(r)\frac{R^2}{r^2}\right) \frac{r}{\sqrt{r^2 - R^2}} dr. \quad (11)$$

N-body models suggest that the orbits of galaxies should be similar to that of the full dark matter distribution, with some deficiency of radial orbits which are selectively removed due to merging and tidal destruction (Ghigna, et al. 1998). In principle, the velocity ellipsoid is constrained by the pvdf, shown in Figure 13.

We model the radial velocity dispersion as

$$\sigma_r^2(r) = \frac{Br}{b+r}, \quad (12)$$

which is a solution of Jeans equation which worked well for clusters (Carlberg Yee & Ellingson 1997). In the absence of other information, the velocity anisotropy,  $\beta = 1 - \sigma_\theta^2/\sigma_r^2$ , is best taken to be a constant independent of radius. However, that choice immediately leads to the somewhat surprising result that the mass-to-light ratio rises with radius. In order to investigate the sensitivity of the result to the velocity anisotropy we adopt the model,

$$\beta(r) = \beta_0 w(r) + \beta_\infty [1 - w(r)], \quad (13)$$

where  $w(r) = r_\beta^2/(r_\beta^2 + r^2)$ . This  $\beta(r)$  function goes to  $\beta_0$  at the origin and  $\beta_\infty$  at large radius. As reasonable alternatives we set  $r_\beta = 0.1r_{200}$  or  $0.3r_{200}$ . This parameter could in principle be part of the nonlinear fit, but because dynamical problems are under-constrained without some knowledge of the velocity anisotropy we choose to use values of this parameter where our  $\beta(r)$  gives a useful variation over the range of the data. The fits are shown for the three different velocity cutoffs in Figure 10. Note that the results for different  $\beta$  are essentially indistinguishable, and that the model has little difficulty giving a statistically acceptable fit to the data.

## 6. The Rising Mass-to-Light Ratio

The dynamical mass profile can be derived from the tracer density profile,  $\nu(r)$ , its velocity dispersion,  $\sigma_r(r)$ , and the velocity anisotropy,  $\beta(r)$ , using Jeans' equation,

$$M(r) = -\frac{\sigma_r^2 r}{G} \left[ \frac{d \ln \sigma_r^2}{d \ln r} + \frac{d \ln \nu}{d \ln r} + 2\beta \right]. \quad (14)$$

The validity of this equation does not rely on  $\nu(r)$  being distributed like the mass density,  $\rho(r)$ . It does require that the system be in dynamical equilibrium, which our group selection procedures



are specifically designed to pick out. Throughout we will use  $L(r) = 4\pi \int \nu r^2 dr$  as the luminosity profile, assuming galaxies have the same mean luminosities at all radii. Strictly speaking we are working out the mass-to-number ratio. The assumption that low and high luminosity galaxies are similarly distributed relative to the mass field is explicitly tested below. The advantage of this approach is that it weights the galaxies relatively equally, rather than concentrating most of the statistical weight on the high luminosity galaxies.

In Figure 14 we display the  $M(r)/L(r)$  profile for the standard group centers with the velocity dispersion calculation cutoff set at three velocity units. Note that this shows the integrated interior  $M/L$ , not the local values. We first model these standard groups using a conventional approach with minimal anisotropy. That is, the central velocity ellipsoid is isotropic, *i.e.*  $\beta_0 = 0$ , the anisotropy radius,  $r_\beta$ , is at about the midpoint of the virialized region,  $r_\beta = 0.3r_{200}$ . The outer anisotropy,  $\beta_\infty$ , takes on the values  $-1, -\frac{1}{2}, 0$  and  $\frac{1}{4}$ , which range from nearly tangential to slightly radial velocity anisotropy. The  $M/L$  curves are normalized to unity at the data point closest to  $r/r_{200} = 1$ . The data indicate about a factor of three to ten rise in the mass-to-light per decade of radius, with little sensitivity to the outer velocity anisotropy. That is, the light is much more centrally concentrated than the mass. This effect is visible for many of the groups where their sky distribution is much more concentrated than their  $r_{200}$  as shown in Figure 6.

The insets in Figure 14 address the concern about erroneously large  $\sigma_1$  values biasing the properties of the mean groups. The lower inset shows the results of the analysis based on the stacked groups restricted to have  $\sigma_1 \leq 200 \text{ km s}^{-1}$ . The upper inset is the result of the analysis where we have overlaid all groups in physical co-ordinates. For convenience and comparability in this case we have taken  $\sigma_1 = 200 \text{ km s}^{-1}$  for the scaling. Although there are differences in the details of the result  $M/L$  curves the rising trend is preserved. Overlaying groups in physical space serves to minimize the size of the rise. The differences between these results serves as an indication of the size of the systematic errors.

The mass-density profile,  $\rho(r)$ , derived from the mass profile as  $(4\pi r^2)^{-1}dM/dr$ , is plotted in Figure 15 for the same models as in Figure 14. The model with the most extreme velocity ellipsoid at large radii, the tangentially dominant  $\beta_\infty = -1$  (solid line), implies a large core which becomes relatively smaller as  $\beta_\infty$  becomes more positive. This model dependent result is one of the most interesting aspects of these groups and its reality needs to be tested which we can at least partially do within our own data. The upper and lower insets are for the  $\sigma_1 \leq 200 \text{ km s}^{-1}$  sample and the physical co-ordinate stacking of the entire sample, respectively.

An alternate version of the groups, with  $r_z^{max} = 3h^{-1} \text{ Mpc}$ , is analyzed in the same way as the  $r_z^{max} = 5h^{-1} \text{ Mpc}$  groups with mass-to-light shown in the upper left panel of Figure 16 and density in Figure 17. In this case, an even steeper rise of mass-to-light emerges than for the standard groups. For velocity ellipsoids with  $\beta_\infty > -1$  the central mass density is negative. The effect of analyzing the standard groups with  $r_\beta = 0.1r_{200}$  is shown in the upper right panels of Figures 16 and 17. This small  $r_\beta$  boosts the sensitivity of the gradient to  $\beta_\infty$ . We conclude that the existence

of a core in the dark matter distribution depends sensitively on the assumption that the velocity anisotropy is close to isotropic.

A strong tangential anisotropy in the center,  $\beta_0 = -1$ , is able to almost eliminate the mass-to-light gradient as shown in the lower panels of Fig 17, with  $r_\beta = 0.3r_{200}$  (left) and  $r_\beta = 0.1r_{200}$  (right). However we recall that the pvdf of Figure 13 does not favor such strong anisotropy. The implied density, shown in the lower left panel of Fig 17, is nearly a power law,  $r^{-2}$ , for  $\beta_\infty = -1$ , and none of these resemble the predicted dark matter density profiles (Navarro, Frenk & White 1996; Moore et al. 1999a).

The source of the rising  $M/L$  in the kinematic data is readily understood. In a power law density distribution with a radial density dependence of  $\rho \propto r^{-2+p}$ , the mass generating the potential must have a velocity dispersion profile of  $\sigma^2 \propto r^p$ . From the velocity dispersion we measure that  $p \simeq \frac{1}{4} \pm \frac{1}{4}$ . This implies a mass density profile that is slightly shallower than  $r^{-2}$ . The measured mean light profile,  $\nu(r) \propto r^{-2+q}$ , with  $q \simeq -\frac{1}{2}$ . Consequently the mass to light ratio,  $\int \rho r^2 dr / \int \nu r^2 dr$ , which varies as  $r^{p-q}$ , rises as  $r^{\frac{3}{4} \pm \frac{1}{4}}$ . Nearly circular orbits can flatten the  $M/L$  profile for the observed velocities, but these  $\beta$  would be very different than the observational results for rich galaxy clusters (Carlberg Yee & Ellingson 1997; van der Marel et al. 2000) and n-body experiments (Ghigna, et al. 1998). One significant difference between groups and rich clusters is that the timescale for dynamical friction to act declines as  $\sigma_1^3$ , so that dynamical friction is much more effective for galaxies orbiting in groups than clusters.

### 6.1. Color and Luminosity Dependent $M/L$ Profiles

As a test of the galaxy population dependence of the result, we divide the group galaxies in to blue and a red subsamples, splitting at  $(B - R)_0 = 1.25$  mag. In a second test we divide the group galaxy sample into high and low luminosity subsamples, splitting at  $M_R^{k,e} = -20$  mag. The resulting  $M/L$  profiles, both masses and luminosity profiles calculated from these subsamples alone, are shown in Figure 18. To simplify the comparison we keep  $\beta_0 = 0$  for all models, but continue to vary  $\beta_\infty$ .

The blue galaxies do a much better job of tracing the mass profile, that is, it is fairly flat, than the red galaxies do. The opposite is true in clusters (Carlberg Yee & Ellingson 1997). In both clusters and groups the red galaxies are more centrally concentrated than the blue galaxies. The  $M/L$  gradient does not have a significant dependence on the luminosities of the galaxies. The latter is an argument that dynamical friction on a galaxy’s gas and stars might not be the dominant source of the segregation of mass and light in groups. However, the presence of a much stronger  $M/L$  gradient for the red galaxies would be consistent with dynamical friction taking several orbits after entry into the cluster to produce a segregation.

## 7. Discussion and Conclusions

In this paper we use the CNOC2 survey catalogues, containing approximately 6000 galaxies with redshifts, to identify more than 200 high probability virialized groups containing, on the average, 3.8 members with redshifts for a total of about 1000 group members. This represents about 25% of all eligible galaxies in the sample. These groups have selection dependent  $M_{VT}/L$  values comparable to the values of large clusters with the “standard” groups being about a factor of two lower. The group population volume density matches on to the number-velocity dispersion relation of clusters. The clustering of groups is enhanced at about the level expected for the approximately 200  $\text{km s}^{-1}$  velocity dispersion dark matter halos of groups as compared to the approximately 100  $\text{km s}^{-1}$  halos of individual galaxies. Overall the global properties of groups are about as expected for dark matter halos on this mass scale.

Quite unlike rich clusters which have a mass-to-light profile constant with radius (Carlberg Yee & Ellingson 1997), our analysis of the internal properties of galaxy groups finds considerable evidence for a gently rising mass-to-light profile with radius. A second difference is that in groups the blue galaxies follow the dark mass more closely than the red galaxies. This paper presents several lines of argument that the rising velocity dispersion profile with radius is not an artifact of the analysis. Moreover, the projected velocity distribution function indicates that the orbital distribution is unlikely to consist almost entirely of circular orbits, as would be required to minimize the rise in  $M/L$  with radius.

The inference that  $M/L$  rises with radius depends sensitively on the theoretical and indirect observational indication that the mean velocity ellipsoid is approximately isotropic. Hence this result needs to be independently verified. Current indirect support for this result comes from X-ray observations of low redshift galaxy groups having velocity dispersion overlap with our sample near 300  $\text{km s}^{-1}$ . The X-ray emission is significantly more extended than most of the group light indicating a rising  $M/L$  (Kriss Cioffi & Canizares 1983; Mulchaey & Zabludoff 1998). Weak gravitational lensing is one of the best prospects to check this result since it has no dependence on assumptions of equilibrium. These intermediate redshift groups are ideally situated for weak lensing studies (Hoekstra et al. 2000). The somewhat puzzling weak lensing results for the low velocity dispersion cluster MS1224+20 in two independent studies indicates that the  $M/L$  is rising with radius (Fahlman Kaiser Squires & Woods 1994; Carlberg 1994; Fischer 1999). Given the large group to group fluctuations it will be important to examine a statistically meaningful sample.

A highly model dependent result is that we find that the mean group most likely has a significant core radius. To retain a power law form would require very tangential orbits near the center. However, a large core could simply be a trivial result of the group galaxies sloshing around in the group potential, such that the centers of light and mass are not coincident. To further investigate the location and radial dependence of the central density profile of groups will require studying individual groups in detail, possibly with X-ray and weak lensing measurements.

What is the origin of the rising  $M/L$ ? The two physical possibilities are that galaxies sink

with respect to the dark matter, or, that group dark matter has a small effective pressure which does not allow the core to undergo the same gravitational collapse as cold collisionless matter can. It is important to note that near  $r_{200}$  both the galaxies and the dark matter have undergone about the same amount of collapse relative to the field. It is only in the inner third or so where the major differences develop, and the size of those differences is strongly dependent on the kinematic model. The simplest explanation is that these observations confirm the standard picture of a collisionless dark matter with gaseous dissipation allowing the baryonic matter to concentrate to the center of individual dark matter halos. As galaxies cluster together to form a group their individual halos are tidally removed to join the common halo from the outside in. Dynamical friction from the collisionless dark matter causes the galaxies to sink in the common group halo, over about a Hubble time (Barnes 1985; Mamon 1987; Evrard 1987; Bode Cohn & Lugger 1993; Pildis Evrard & Bregman 1996). One possible concern with this interpretation is that when groups join together to make rich clusters this history needs to be erased to leave no measurable  $M/L$  gradient. Furthermore, whether this mechanism is consistent with no luminosity dependence of the  $M/L$  gradient but a large galaxy color dependence of the  $M/L$  gradient puts some fairly strong, but not necessarily unreasonable constraints, on the formation history of the galaxies.

A more extreme possibility for the origin of the  $M/L$  gradient is that the dark matter is subject to some effective pressure that does not allow it to undergo full gravitational collapse to form a core, either through a phase density limit, or through collisional interactions (Spergel & Steinhardt 1999). More conventional explanations should be carefully examined and our results independently verified with other methods of observation before this is accepted.

This research was supported by NSERC and NRC of Canada. HL acknowledges support provided by NASA through Hubble Fellowship grant #HF-01110.01-98A awarded by the Space Telescope Science Institute, which is operated by the Association of Universities for Research in Astronomy, Inc., for NASA under contract NAS 5-26555. We thank the CFHT Corporation for support, and the operators for their enthusiastic and efficient control of the telescope.

## REFERENCES

- Abell, G. O. 1958 ApJS, 3, 211
- Avila-Reese, V. , Firmani, C. , Klypin, A. & Kravtsov, A. V. 1999, MNRAS, 310, 527
- Bardeen, J. M., Bond, J. R., Kaiser, N. & Szalay, A. S. 1986, ApJ, 304, 15
- Barnes, J. 1985, MNRAS, 215, 517
- Bode, P. W., Cohn, H. N., & Lugger, P. M. 1993, ApJ, 416, 17
- Borgani, S., Girardi, M., Carlberg, R. G., Yee, H. K. C. and Ellingson, E. 1999, ApJ, 527, 561
- Burbidge, E. M.& Burbidge, G. R. 1961, AJ, 66. 541
- Carlberg, R. G. 1994, ApJ, 434, L51
- Carlberg, R. G., Yee, H. K. C., Ellingson, E., Abraham, R., Gravel, P., Morris, S. & Pritchett, C. J. 1996, ApJ, 462, 32
- Carlberg, R. G., et al. 1997, ApJ, 485, L13
- Carlberg, R. G., Yee, H. K. C., & Ellingson, E. 1997, ApJ, 478, 462
- Carlberg, R. G., Morris, S. L., Yee, H. K. C. & Ellingson, E. 1997, ApJ, 479, L19
- Carlberg, R. G., and 13 colleagues 2000, ApJ, 532, L1
- Carlberg, R. G., Yee, H. K. C., Morris, S. L., Lin, H. Hall, P. B., Patton, D., Sawicki, M. & Shepherd, C. W. 2000, ApJ, in press (astro-ph/9910250)
- Davis, M. & Peebles, P. J. E. 1983, ApJ, 267, 465
- Dubinski, J. & Carlberg, R. G. 1991, ApJ, 378, 496
- Efstathiou, G., Bond, J. R. & White, S. D. M. 1992, MNRAS, 258, 1P
- Eke, V. R., Navarro, J. F. & Frenk, C. S. 1998, ApJ, 503, 569
- Evrard, A. E. 1987, ApJ, 316, 36
- Fahlman, G., Kaiser, N., Squires, G. and Woods, D. 1994, ApJ, 437, 56
- Fischer, P. 1999, AJ, 117, 2024
- Ghigna, S., Moore, B., Governato, F., Lake, G., Quinn, T. and Stadel, J. 1998, MNRAS, 300, 146
- Girardi, M. , Boschin, W. & da Costa, L. N. 2000, A&A, 353, 57

- Girardi, M. & Giuricin, G. 2000, ApJ, in press (astro-ph/0004149)
- Gott, J. R. , III & Turner, E. L. 1976, ApJ, 209, 1
- Governato, F., Baugh, C. M., Frenk, C. S., Cole, S., Lacey, C. G., Quinn, T. & Stadel, J. 1998, Nature, 392, 359
- Heisler, J., Tremaine, S. and Bahcall, J. N. 1985, ApJ, 298, 8
- Hickson, P. 1982, ApJ, 255, 382
- Hoekstra, H. *et al.* 2000, in preparation.
- Jing, Y. P. 1998, ApJ, 503, L9
- Kaiser, N. 1984, ApJ, 284, L9
- Kaiser, N. 1987, MNRAS, 227, 1
- Kriss, G. A., Cioffi, D. F. & Canizares, C. R. 1983, ApJ, 272, 439
- Lin, H., Yee, H. K. C., Carlberg, R. G., Morris, S. L., Sawicki, M., Patton, D., Wirth, G. & Shepherd, C. W. 1999, ApJ, 518, 533
- Mamon, G. A. 1987, ApJ, 321, 622
- Mo, H. J. & White, S. D. M. 1996, MNRAS, 282, 347
- Moore, B., Frenk, C. S. & White, S. D. M. 1993, MNRAS, 261, 827
- Moore, B., Quinn, T., Governato, F., Stadel, J. & Lake, G. 1999a, MNRAS, 310, 1147
- Moore, B. , Ghigna, S. , Governato, F. , Lake, G. , Quinn, T. , Stadel, J. & Tozzi, P. 1999b, ApJ, 524, L19
- Mulchaey, J. S. & Zabludoff, A. I. 1998, ApJ, 496, 73
- Navarro, J. F., Frenk, C. S. & White, S. D. M. 1996, ApJ, 462, 563
- Nolthenius, R. & White, S. D. M. 1987, MNRAS, 225, 505
- Peebles, P. J. E. 1980, *Large Scale Structure of the Universe* (Princeton University Press: Princeton)
- Pildis, R. A., Evrard, A. E. & Bregman, J. N. 1996, AJ, 112, 378
- Press, W. H. & Schechter, P. 1974, ApJ, 187, 425
- Press, W. H., Teukolsky, S. A., Vetterling, W. T., & Flannery, B. P. 1992, *Numerical Recipes in C* (Cambridge University Press)

- Ramella, M. , Geller, M. J. & Huchra, J. P. 1990, ApJ, 353, 51
- Spergel, D. N. & Steinhardt, P. J. 2000, Physical Review Letters (in press) (astro-ph/9909386)
- Shectman, S. A., Landy, S. D., Oemler, A., Tucker, D. L, Lin, H., Kirshner, R. P. & Schechter, P. L. 1996, ApJ, 470, 172
- van der Marel, R. P., Magorrian, J., Carlberg, R. G., Yee, H. K. C. & Ellingson, E. 2000, AJ, in press (astro-ph/9910494)
- White, S. D. M., Davis, M. , Efstathiou, G. & Frenk, C. S. 1987, Nature, 330, 451
- White, S. D. M., Efstathiou, G., & Frenk, C. S. 1993, MNRAS, 262, 1023
- Yee, H. K. C., Ellingson, E., & Carlberg, R. G. 1996, ApJS, 102, 269
- Yee, H. K. C., *et al.* 2000, ApJS, in press (astro-ph/0004026)

Table 1: The  $r_z^{max} = 5h^{-1}$  Mpc,  $r_p^{max} = 0.25h^{-1}$  Mpc Groups

x ''	y ''	z	$\sigma_1$ km s <sup>-1</sup>	M/L h M <sub>⊙</sub> /L <sub>⊙</sub>	N <sub>g</sub> <sup>z</sup>	M h <sup>-1</sup> M <sub>⊙</sub>
0223+00						
-256.4	546.7	0.18809	80± 70	11± 36	3	5.116e+11± 192%
-204.3	1484.6	0.19834	95± 74	58± 324	3	2.303e+12± 127%
1589.7	-1504.7	0.21787	126± 71	41± 61	5	3.443e+12± 100%
-16.2	2522.1	0.22075	65± 68	33± 106	3	1.349e+12± 183%
549.8	-171.4	0.22781	111± 56	39± 56	4	3.995e+12± 73%
382.6	-110.8	0.22920	184± 50	206± 190	4	8.637e+12± 48%
117.7	-395.2	0.26741	254± 104	274± 283	6	2.084e+13± 76%
2367.5	-1396.8	0.27011	134± 38	108± 104	6	5.681e+12± 74%
162.9	1737.6	0.27038	148± 86	262± 433	4	7.775e+12± 101%
2331.2	-1613.0	0.27045	118± 123	104± 214	3	4.478e+12± 137%
218.8	708.6	0.29864	115± 66	30± 44	5	1.704e+12± 94%
-753.8	-146.8	0.30207	375± 85	271± 339	5	3.367e+13± 43%
-44.3	-884.3	0.30275	95± 103	62± 108	3	1.541e+12± 123%
-130.1	2991.5	0.30496	135± 130	51± 68	3	3.504e+12± 115%
132.8	2579.2	0.30520	266± 181	143± 202	5	1.619e+13± 109%
256.6	74.7	0.30647	305± 326	1115±2313	3	3.278e+13± 150%
554.8	64.3	0.30933	95± 73	49± 74	4	2.304e+12± 116%
1198.3	-1408.6	0.33835	92± 53	13± 25	4	1.092e+12± 165%
-105.8	1465.8	0.35084	160± 197	132± 406	3	5.871e+12± 179%
-41.2	-882.2	0.35746	122± 112	46± 92	3	4.951e+12± 113%
-92.1	-736.2	0.35772	154± 150	140± 279	4	1.130e+13± 131%
450.5	-386.1	0.35811	574± 483	1557±2715	4	1.102e+14± 117%
710.7	-451.5	0.35851	305± 104	120± 139	7	2.441e+13± 74%
608.7	-87.3	0.36049	365± 169	693±1044	5	6.553e+13± 80%
557.6	-226.1	0.36107	202± 68	85± 155	5	1.190e+13± 62%
-396.9	-324.0	0.36464	265± 203	289± 498	3	3.008e+13± 92%
929.9	-1595.8	0.38473	362± 218	287± 371	5	4.703e+13± 88%
-642.4	-609.8	0.38483	180± 193	131± 345	3	8.168e+12± 196%
1016.4	-856.2	0.38644	228± 173	119± 155	6	1.500e+13± 104%
631.4	-1119.5	0.38661	229± 165	107± 172	4	1.064e+13± 128%
102.1	2003.8	0.39651	216± 42	127± 84	6	1.780e+13± 35%
1639.8	-1625.9	0.39654	645± 443	2439±6437	3	1.521e+14± 191%
-102.1	609.7	0.39715	261± 211	264± 484	3	2.087e+13± 103%
-167.6	2053.8	0.39785	230± 174	207± 170	4	2.036e+13± 76%
89.5	1582.7	0.40166	191± 92	128± 164	4	1.475e+13± 66%
233.2	1396.3	0.40494	667± 479	3266±14005	3	1.799e+14± 252%
695.3	-1015.4	0.40785	459± 141	277± 370	5	7.083e+13± 54%



x "	y "	z	$\sigma_1$ km s <sup>-1</sup>	M/L h M <sub>⊙</sub> /L <sub>⊙</sub>	N <sub>g</sub> <sup>z</sup>	M h <sup>-1</sup> M <sub>⊙</sub>
0223+00						
566.7	-232.9	0.40816	444± 522	551±1976	3	6.454e+13± 231%
464.6	197.9	0.41259	234± 247	134± 196	3	1.003e+13± 126%
56.1	2154.8	0.41916	183± 60	140± 124	5	1.484e+13± 50%
-171.5	2316.5	0.44237	86± 94	46± 132	3	2.524e+12± 171%
29.0	3007.5	0.46898	197± 142	64± 192	3	1.091e+13± 92%
177.0	2967.2	0.47066	79± 58	8± 28	3	7.906e+11± 177%
0920+37						
-243.5	14.5	0.19117	253± 129	215± 550	5	1.928e+13± 104%
182.0	1070.6	0.19149	99± 82	82± 230	3	3.290e+12± 109%
130.7	-604.8	0.20203	108± 104	67± 299	3	3.422e+12± 284%
-526.3	-1112.5	0.20227	143± 163	124± 277	3	3.418e+12± 146%
0.5	1098.7	0.20714	262± 170	150± 343	4	1.120e+13± 108%
2342.2	-1435.5	0.22135	392± 120	299± 375	8	4.539e+13± 70%
2294.1	-1439.0	0.22476	164± 96	168± 302	4	1.029e+13± 96%
2406.8	-1450.4	0.22506	182± 188	342±1308	3	1.077e+13± 130%
2339.5	-1290.9	0.22556	213± 255	509±1235	3	1.584e+13± 170%
-172.0	89.5	0.23083	83± 54	24± 40	4	2.096e+12± 114%
31.2	-266.9	0.23299	197± 146	306± 889	3	1.046e+13± 96%
-200.0	-673.6	0.24328	157± 104	223± 423	4	7.858e+12± 105%
-325.3	-274.7	0.24347	202± 107	598± 947	4	1.665e+13± 90%
-166.2	189.2	0.24395	148± 43	90± 132	6	7.245e+12± 59%
-17.3	931.5	0.24438	185± 49	235± 192	6	1.242e+13± 56%
303.9	103.3	0.24441	158± 27	81± 52	7	6.221e+12± 42%
-40.4	-388.1	0.24447	125± 105	210± 866	3	4.561e+12± 256%
-258.2	308.6	0.24500	348± 329	1209±2431	3	3.154e+13± 118%
151.1	1534.7	0.24515	297± 195	482±1684	4	2.833e+13± 94%
-126.4	2379.0	0.24535	226± 97	145± 157	5	1.272e+13± 79%
91.4	1894.1	0.24611	263± 58	337± 351	5	2.289e+13± 46%
-607.9	178.4	0.24623	147± 47	58± 83	6	4.670e+12± 73%
178.9	280.5	0.24763	190± 107	199± 406	4	1.366e+13± 119%
1315.8	-902.3	0.25424	97± 78	35± 180	3	2.415e+12± 378%
36.6	749.5	0.25955	192± 139	114± 176	6	1.369e+13± 119%
983.1	-1531.8	0.28641	72± 60	25± 69	3	4.023e+11± 169%
61.6	693.3	0.31835	427± 473	3073±8122	3	9.172e+13± 152%
381.8	-149.0	0.32181	144± 176	205± 649	3	5.857e+12± 181%
-145.8	1587.5	0.32201	111± 93	33± 117	3	2.974e+12± 113%
74.4	1020.4	0.32273	167± 149	136± 367	4	9.154e+12± 170%

x "	y "	z	$\sigma_1$ km s <sup>-1</sup>	M/L h M <sub>⊙</sub> /L <sub>⊙</sub>	N <sub>g</sub> <sup>z</sup>	M h <sup>-1</sup> M <sub>⊙</sub>
0920+37						
203.4	403.9	0.32380	230± 113	305± 405	4	1.378e+13± 98%
-169.5	1189.9	0.32384	256± 128	472± 543	5	2.173e+13± 92%
-20.4	721.8	0.36173	109± 92	66± 290	3	4.329e+12± 312%
184.0	-816.1	0.36178	412± 507	596±1514	3	3.697e+13± 181%
114.1	2543.7	0.37218	542± 308	838±1372	4	5.252e+13± 117%
-175.3	180.4	0.37237	160± 32	68± 79	4	4.896e+12± 54%
-155.8	-1194.7	0.37247	436± 148	502± 427	6	5.015e+13± 56%
-233.7	-90.2	0.37291	126± 125	75± 128	3	6.057e+12± 123%
-370.3	-888.2	0.37317	328± 210	360± 607	5	4.321e+13± 95%
-119.8	-1090.8	0.37323	251± 85	284± 425	4	1.561e+13± 90%
-376.8	-132.5	0.37331	231± 129	287± 832	4	1.720e+13± 197%
-354.6	-742.9	0.37352	147± 81	60± 81	4	1.194e+13± 127%
-255.8	-962.7	0.37406	86± 82	43± 75	3	2.761e+12± 113%
-218.3	-1056.9	0.37426	639± 154	761± 628	8	1.587e+14± 49%
-102.3	226.3	0.37597	541± 506	1085±2781	3	6.384e+13± 125%
1759.2	-1385.0	0.37893	109± 114	78± 240	3	5.958e+12± 120%
742.9	-481.4	0.37894	353± 246	402±1069	3	2.454e+13± 112%
1036.3	-971.8	0.37903	281± 224	298±1408	3	3.073e+13± 113%
-54.4	661.1	0.37978	91± 102	39± 111	3	2.769e+12± 121%
-366.6	-493.7	0.38032	328± 377	331± 677	3	1.638e+13± 135%
-257.3	1320.1	0.38462	138± 104	82± 206	3	9.262e+12± 177%
383.8	91.6	0.38820	403± 108	492± 542	4	5.753e+13± 55%
900.0	-1302.6	0.38995	232± 191	510±1099	3	3.083e+13± 174%
86.5	426.7	0.39019	158± 122	56± 178	3	4.814e+12± 112%
1720.0	-1718.3	0.39096	184± 195	103± 192	4	1.537e+13± 120%
445.1	201.0	0.39177	86± 54	18± 34	4	2.451e+12± 109%
114.2	112.1	0.39196	209± 166	210± 573	3	1.562e+13± 100%
-381.9	183.6	0.39527	181± 199	142± 200	3	5.827e+12± 122%
569.1	-911.0	0.42748	102± 88	48± 76	3	3.825e+12± 117%
974.2	-1696.5	0.46076	445± 484	270±1094	3	3.673e+13± 125%
-308.3	183.0	0.46254	324± 379	200± 514	3	3.258e+13± 171%
-32.5	-127.0	0.47277	294± 212	201± 430	3	2.731e+13± 156%
-568.7	-193.4	0.47289	108± 100	26± 58	3	2.635e+12± 114%
971.2	-1332.8	0.47318	353± 204	139± 223	4	3.848e+13± 93%
1447+09						
-62.1	-334.7	0.16531	164± 126	322± 462	3	1.263e+13± 126%
-28.5	840.0	0.19733	233± 170	318± 543	4	1.466e+13± 136%

x "	y "	z	$\sigma_1$ km s <sup>-1</sup>	M/L h M <sub>⊙</sub> /L <sub>⊙</sub>	N <sub>g</sub> <sup>z</sup>	M h <sup>-1</sup> M <sub>⊙</sub>
1447+09						
-134.2	1877.9	0.20204	326± 360	1328±3276	3	2.271e+13± 151%
155.4	1998.1	0.20249	250± 87	190± 438	4	1.066e+13± 168%
-207.0	2461.4	0.22454	256± 280	248±1706	3	1.527e+13± 140%
12.6	1767.1	0.22854	268± 107	811±1911	4	3.147e+13± 102%
-120.9	1254.9	0.22893	81± 98	37± 93	3	2.308e+12± 165%
629.1	26.7	0.22897	162± 139	325±1186	3	7.214e+12± 113%
595.9	-676.4	0.26162	229± 77	239± 668	4	1.156e+13± 49%
142.6	-986.1	0.26981	104± 92	119± 378	3	2.983e+12± 132%
361.6	-1090.1	0.27057	112± 66	68± 132	4	3.020e+12± 118%
522.3	-1144.8	0.27177	280± 143	347± 399	6	1.969e+13± 85%
-90.6	-641.5	0.27286	165± 120	241± 732	3	8.104e+12± 110%
-693.8	189.9	0.28246	231± 116	187± 318	5	1.367e+13± 80%
728.2	-632.0	0.30639	93± 65	34± 126	3	1.329e+12± 309%
-622.3	-135.7	0.30643	199± 161	228± 653	4	1.598e+13± 103%
1091.1	-1288.5	0.31031	83± 85	6± 29	3	6.854e+11± 443%
1257.0	-775.6	0.32378	180± 149	181± 375	4	8.494e+12± 145%
-526.0	-639.8	0.32506	175± 151	125± 214	4	9.875e+12± 114%
-241.0	655.4	0.32716	247± 148	144± 232	5	1.542e+13± 96%
-216.5	1827.7	0.34855	136± 70	50± 76	6	4.741e+12± 113%
-98.0	1364.0	0.35043	168± 169	200± 377	3	8.209e+12± 120%
158.1	1350.7	0.35062	250± 243	147± 239	3	1.893e+13± 126%
517.5	-83.8	0.35914	82± 66	16± 27	4	1.646e+12± 127%
-80.2	306.3	0.36192	170± 95	131± 183	5	9.828e+12± 120%
-432.0	197.2	0.36404	77± 94	41± 108	3	1.946e+12± 173%
-38.7	-364.1	0.37225	126± 94	69± 153	3	2.787e+12± 131%
-661.0	-422.0	0.37263	44± 41	4± 9	4	2.115e+11± 154%
-166.4	-1015.4	0.37389	291± 193	792±1798	4	3.386e+13± 158%
-338.2	-1151.5	0.39369	308± 257	438± 535	4	3.596e+13± 110%
359.7	174.4	0.39369	394± 406	864±1972	3	4.819e+13± 137%
-256.3	-726.8	0.39438	507± 469	1254±2636	3	7.807e+13± 114%
51.3	1236.2	0.40653	101± 86	54± 76	3	3.620e+12± 103%
836.6	-1022.5	0.46575	150± 146	118± 215	3	6.751e+12± 122%
81.2	-278.7	0.46820	488± 417	668±1154	4	7.482e+13± 125%
124.3	48.3	0.46930	217± 224	78± 166	4	8.894e+12± 141%
101.0	-194.4	0.47168	123± 99	40± 70	3	4.871e+12± 121%
217.5	-572.5	0.51077	565± 668	767±1710	3	1.237e+14± 149%
169.5	1282.7	0.53680	520± 203	477± 625	5	1.355e+14± 72%
213.1	-782.7	0.54249	151± 132	63± 197	3	8.662e+12± 177%

x "	y "	z	$\sigma_1$ km s <sup>-1</sup>	M/L h M <sub>⊙</sub> /L <sub>⊙</sub>	N <sub>g</sub> <sup>z</sup>	M h <sup>-1</sup> M <sub>⊙</sub>
2148-05						
116.4	2726.2	0.15480	257± 76	211± 598	6	2.419e+13± 71%
-14.8	2646.0	0.15649	241± 129	164± 298	4	2.631e+13± 102%
-181.0	-992.4	0.17776	173± 193	167± 490	3	6.127e+12± 124%
32.9	-660.2	0.17803	238± 182	767±1765	3	3.069e+13± 100%
119.0	949.8	0.19828	267± 313	356±1741	3	1.482e+13± 439%
-181.8	3095.2	0.21406	152± 111	306± 611	3	1.124e+13± 111%
-377.8	11.8	0.21926	275± 81	273± 317	7	2.267e+13± 65%
-258.5	-163.1	0.21940	192± 69	96± 80	6	5.039e+12± 71%
-235.8	151.0	0.21941	160± 31	34± 51	7	7.099e+12± 52%
-486.0	-218.9	0.21964	96± 45	30± 75	4	1.494e+12± 111%
452.9	-1101.2	0.23645	121± 90	73± 224	3	3.969e+12± 218%
-765.5	-98.4	0.24135	149± 38	46± 59	5	3.683e+12± 41%
-179.3	1552.7	0.24322	274± 168	316±1951	4	3.163e+13± 108%
-134.4	2245.3	0.24344	146± 114	113± 174	3	7.044e+12± 124%
466.5	-833.0	0.26489	306± 176	261± 334	6	3.355e+13± 90%
206.1	2896.4	0.28672	150± 74	111± 152	4	9.487e+12± 65%
57.6	2932.0	0.28792	144± 114	217± 751	3	9.609e+12± 201%
-783.8	-1131.2	0.30139	70± 50	60± 91	3	1.205e+12± 93%
1787.9	-1515.6	0.31265	103± 37	18± 27	5	1.161e+12± 76%
177.5	2693.2	0.31704	357± 394	853±1720	4	6.038e+13± 152%
333.2	-417.7	0.31759	272± 318	173± 260	3	8.104e+12± 123%
-384.7	-1033.5	0.33391	131± 117	141± 445	3	6.826e+12± 219%
2210.9	-1328.6	0.35762	302± 230	705±1242	4	5.002e+13± 133%
649.6	-489.7	0.35986	358± 428	1182±3100	3	4.096e+13± 162%
466.6	-278.1	0.37338	174± 192	269± 394	3	1.064e+13± 124%
750.2	-472.6	0.39222	134± 107	49± 182	3	2.890e+12± 213%
2195.1	-1708.2	0.39364	214± 142	207± 379	4	1.986e+13± 108%
-3.6	2305.5	0.39380	153± 181	41± 99	3	5.103e+12± 140%
634.7	241.2	0.42607	129± 104	7± 14	4	1.492e+12± 151%
517.2	-474.9	0.44011	620± 314	915± 762	4	1.662e+14± 60%
827.2	-1016.7	0.44041	208± 212	134± 293	3	2.160e+13± 166%
555.6	305.8	0.46596	129± 109	25± 56	3	3.308e+12± 167%

Fig. 1.— The line of sight velocity dispersion as estimated on the first pass (abscissa) of the group refinement and on the fourth pass (ordinate) for sets of group finding parameters. The  $r_p^{max}$  is fixed at  $0.25h^{-1}$  Mpc. The asterisks, circles, x’s and squares are for  $r_z^{max}$  of  $3, 5, 7$  and  $10h^{-1}$  Mpc, respectively.

Fig. 2.— The redshift distribution of groups found with  $r_p^{max}$  fixed at  $0.25h^{-1}$  Mpc and  $r_z^{max}$  (indicated on the figure in the upper right) varying over the same range as Figure 1 .

Fig. 3.— The median  $M/L$  value of the groups versus the fractional spread between the first and third quartile  $M/L$  values. Squares indicate  $r_p^{max} = 0.5h^{-1}$  Mpc groups and circles indicate  $r_p^{max} = 0.25h^{-1}$  Mpc groups. The numbers in the symbols give the values of  $r_z^{max}$ .

Fig. 4.— The mass-to-light ratios of the groups as a function of their velocity dispersions for  $r_p^{max} = 0.25h^{-1}$  Mpc and  $r_z^{max} = 5h^{-1}$  Mpc. The  $1\sigma$  error flags plotted are Jackknife technique estimates. The correlation is the result of the  $\sigma_1^2$  dependence of  $M_{VT}$ . The inset restricts the sample to groups with six or more members.

Fig. 5.— The distribution of measured line-of-sight velocity dispersions in  $100 \text{ km s}^{-1}$  bins, plotted at the bin centers. The parameters for the group selection are indicated by the symbols in the diagram. The dotted line shows the Press-Schechter prediction for the distribution using the cluster normalization.

Fig. 6.— The  $xy$  locations of field galaxies (open circles) and group galaxies (filled), along with  $r_{200}$  radii of the groups found between redshifts 0.1 and 0.45 in the 0223+00 field. The starting parameters are  $r_p^{max} = 0.25h^{-1}$  Mpc and  $r_z^{max} = 5h^{-1}$  Mpc (co-moving). The group members are marked with filled symbols. Note that the group members fill their  $r_{200}$  to varying degrees. None of the members are outside the estimated region of virialization estimated for a low density universe,  $1.5r_{200}$ . The major ticks are at intervals of 1000 arcsec, with North up and East to the left.

Fig. 7.— The redshift space (open circles) and projected real space (filled diamonds) correlations for the  $r_p^{max} = 0.25h^{-1}$  Mpc and  $r_z^{max} = 5h^{-1}$  Mpc groups. The errors here are simply the square root of the pair count in the bin. The fitted correlation lengths are  $6.8 \pm 0.3h^{-1}$  Mpc and  $6.5 \pm 0.3h^{-1}$  Mpc, respectively.

Fig. 8.— The scaled radius versus the source group’s velocity dispersion for all galaxies in the mean group for  $\Delta v^{max} = 3\sigma_1$  prior to statistical background subtraction. The small plus signs are for all galaxies contributing to the mean group whereas the filled octagons mark the galaxies identified as group members using our algorithm.

Fig. 9.— The number weighted surface density of galaxies in the mean group. The points and three fitted lines show the slow *decrease* of the normalized surface density at intermediate radii with clipping at 3, 4 and 5 velocity units. The inset shows  $\Sigma_N(R)$  using only the  $\sigma_1 \leq 200 \text{ km s}^{-1}$  groups with (solid line) and, for reference, all velocity dispersion groups cutoff again (dotted line),

both with 3 velocity unit clipping.

Fig. 10.— The number-weighted projected velocity dispersion profile. The circle, cross and square are for velocity cuts at 3, 4 and 5 velocity unit cutoff, which are fit by the solid line and the dashed and dotted lines (which are hard to distinguish because they are overlaid).

Fig. 11.— The number-weighted projected velocity dispersion profile for alternate values of  $r_z^{max}$  of 2, 3, 7 and 10  $h^{-1}$  Mpc. The circle, cross and square are for velocity cuts at 3, 4 and 5 velocity units, and fitted by solid, dashed and dotted lines, respectively.

Fig. 12.— The mean radially normalized group in position and velocity,  $\xi(R, \Delta v)/\Sigma(r_p)$ , selected using  $r_p^{max} = 0.25h^{-1}$  Mpc and  $r_z^{max} = 5h^{-1}$  Mpc. Each column of fixed  $R$  is normalized to a total of unity. The gray scale is proportional to the logarithm of the local over-density in the normalized velocity and radius. The second moment of this distribution in the vertical direction is  $\sigma_p(R)$  of Figure 10. The lowest over-density value (white) is 0.2% of the total, and the highest (black) is 10% of the total in the entire  $R$  bin.

Fig. 13.— The projected velocity distribution function (pvdF), normalized to have unit velocity dispersion and unit area under the curve. The pvdF for cutoffs of 3 and 4 velocity units are shown as solid and short dashed stepped lines, respectively. The reference lines are a Gaussian and an exponential distribution, solid and short-dashed lines, respectively.

Fig. 14.— The rising mass-to-light ratio from the 3 velocity unit cutoff velocity dispersion profile for group centers identified with  $r_p^{max} = 0.25h^{-1}$  Mpc and  $r_z^{max} = 5h^{-1}$  Mpc. The galaxy co-ordinates are scaled to their groups  $\sigma_1$  and  $r_{200}$ . The errors are computed from the velocity dispersion errors. The upper inset shows the results obtained by overlaying the galaxies in physical co-ordinates assuming  $\sigma_1 = 200 \text{ km s}^{-1}$  and the lower shows the results after restricting the analysis to groups with velocity dispersion less than  $200 \text{ km s}^{-1}$ . The solid, dashed, dot-dashed and dotted lines are for  $\beta_\infty = -1, -\frac{1}{2}, 0,$  and  $\frac{1}{4}$ , respectively

Fig. 15.— The inferred dark matter density profile for the variable velocity anisotropy model, with  $\beta_0 = 0$ ,  $r_\beta = 0.3r_{200}$  and  $\beta_\infty = -1, -\frac{1}{2}, 0$  and  $\frac{1}{4}$  for solid, dashed, dot-dashed and dotted lines, respectively, as in Figure 14. The lower inset shows the results obtained by overlaying the galaxies in physical co-ordinates and the upper shows the results after restricting the analysis to groups with velocity dispersion less than  $200 \text{ km s}^{-1}$ .

Fig. 16.— Profiles of  $M/L$  for an alternate data set,  $r_z^{max} = 3h^{-1}$  Mpc and  $r_p^{max} = 0.25h^{-1}$  Mpc (upper left) and the standard groups sample analyzed with a small  $r_\beta = 0.1r_{200}$  (upper right). In both lower panels we use an extremely tangential velocity ellipsoid,  $\beta_0 = -1$  with the standard  $r_\beta = 0.3r_{200}$  (lower left), and a small  $r_\beta = 0.1r_{200}$ , (lower right). The lines have the same meaning as in Figure 15. When the  $M/L$  has a zero-crossing dip the the implied values of the mass are negative at small radii. These show that a nearly tangential velocity ellipsoid can eliminate the inference of a rising mass-to-light ratio.

Fig. 17.— The density profiles for the data and models of Figure 16. Again, masses are negative at small radii when a zero-crossing dip is present.

Fig. 18.— The inferred mass-to-light ratios (normalized to unity at  $r_{200}$ ) for galaxy subsamples within the groups. The top row has blue (left) and red (right) selected galaxies. The bottom row has high (left) and low (right) luminosity galaxies. The smooth lines show the modeled results. The main result is that blue galaxies trace the mass distribution much more closely than the red galaxies.

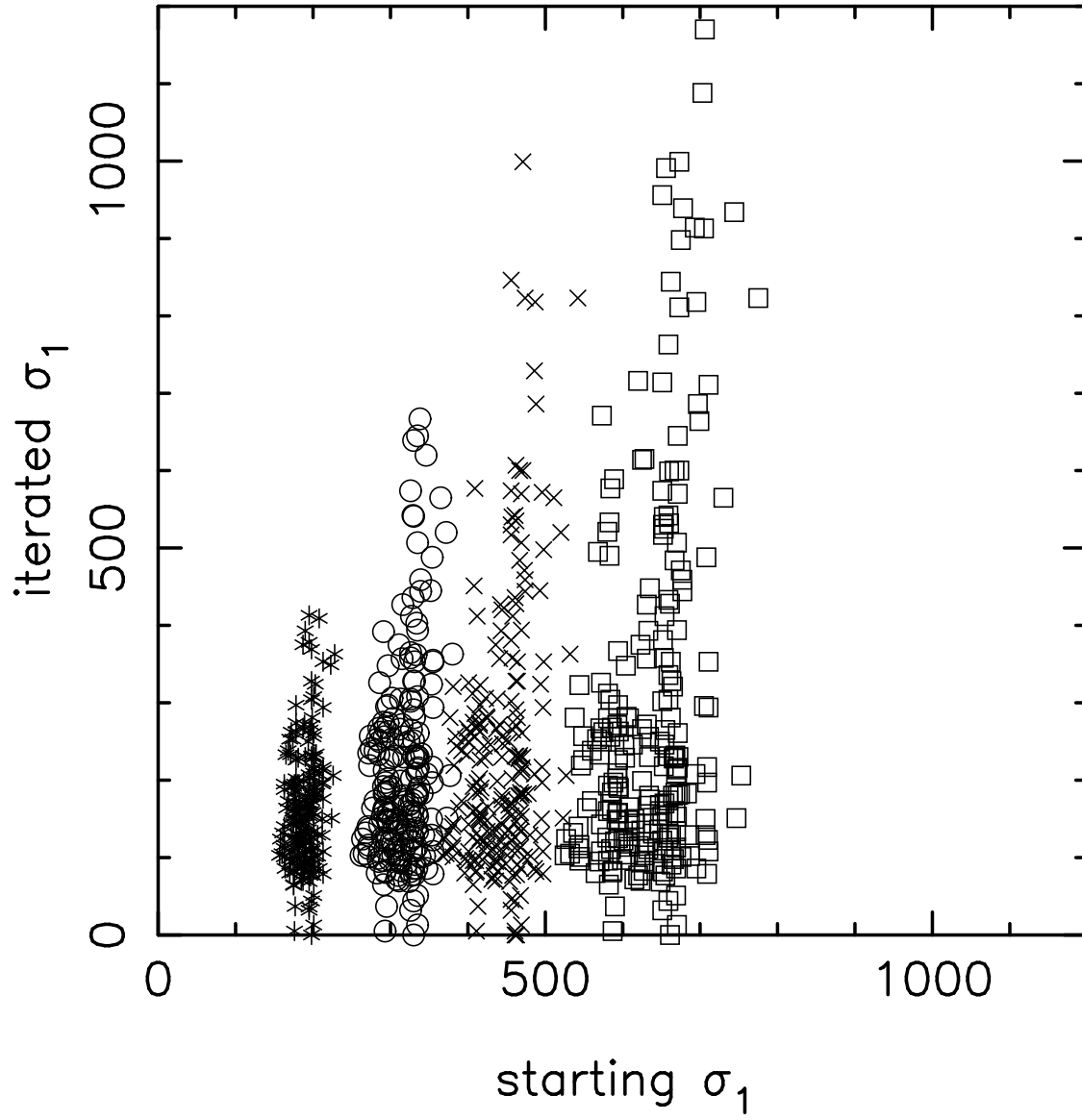


Fig. 1.—



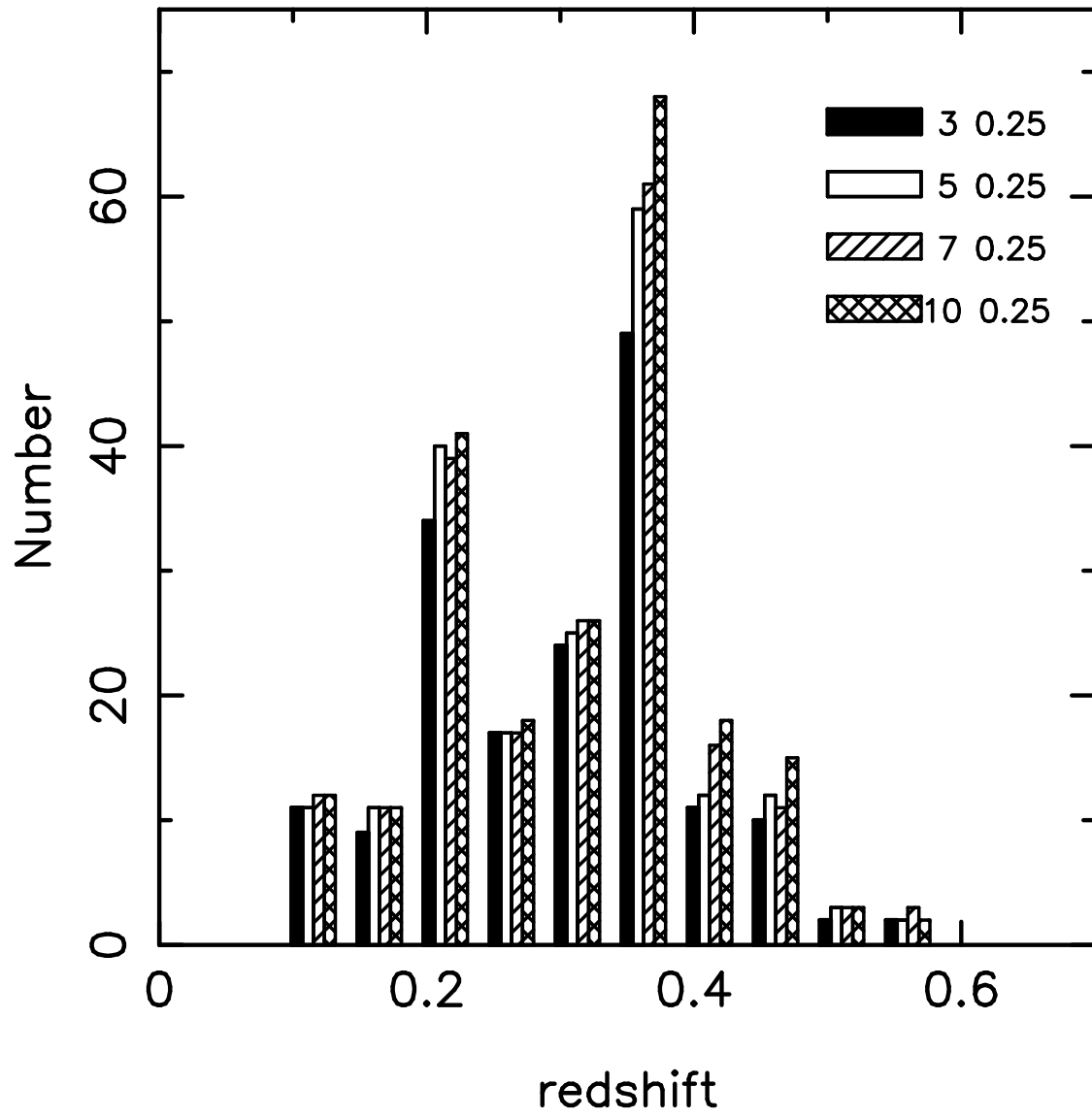


Fig. 2.—

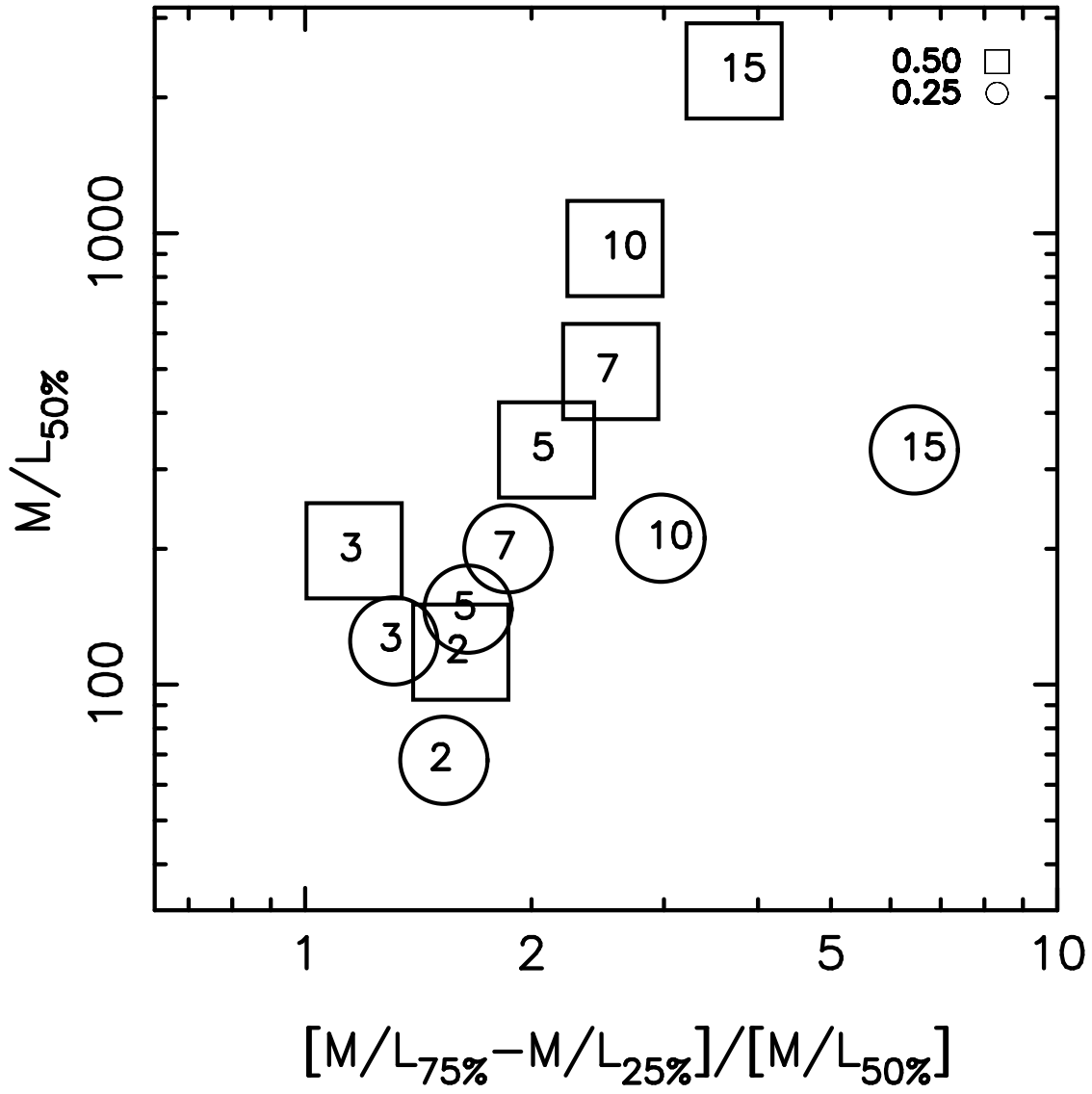


Fig. 3.—

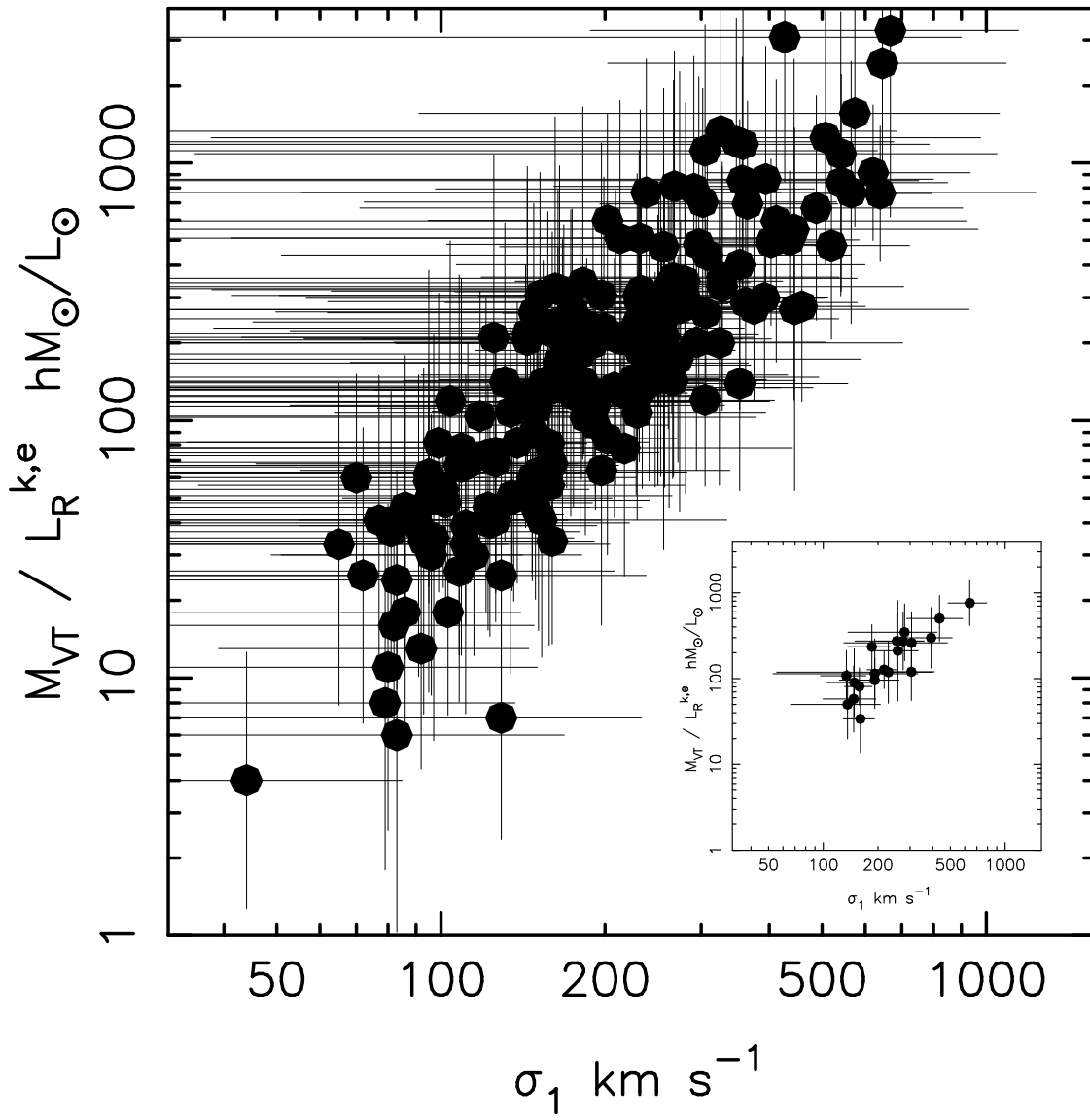


Fig. 4.—

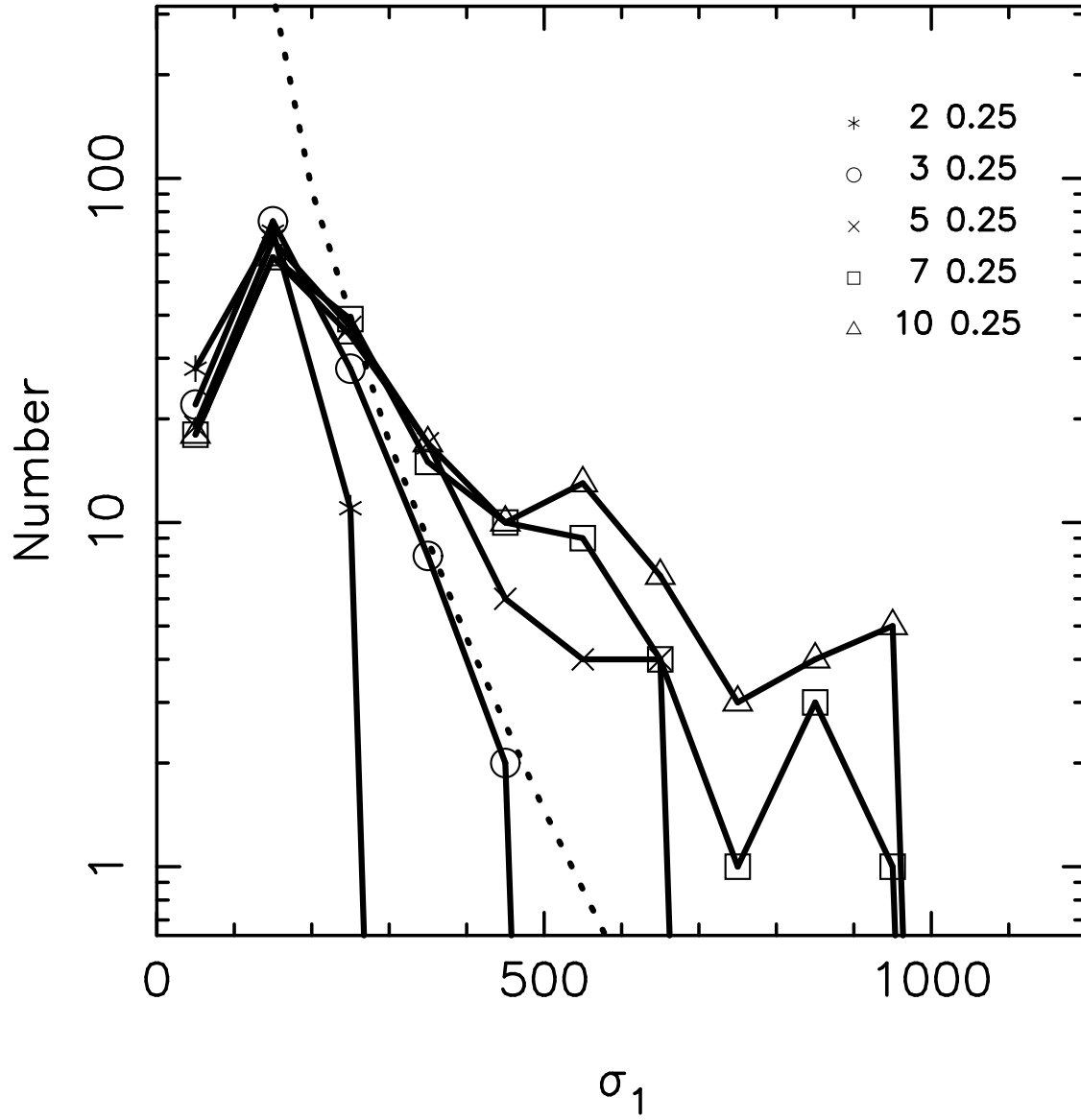


Fig. 5.—

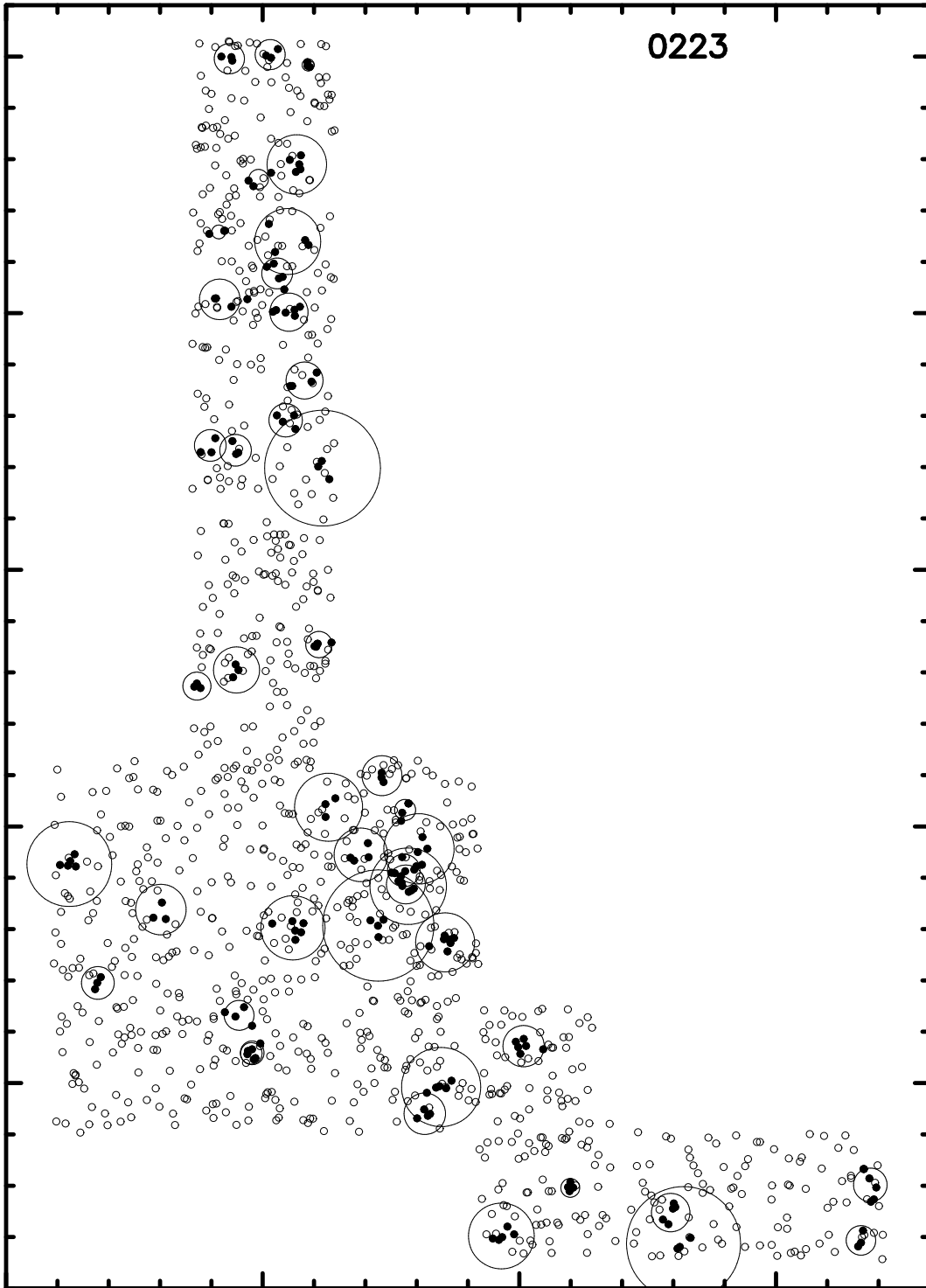


Fig. 6.—

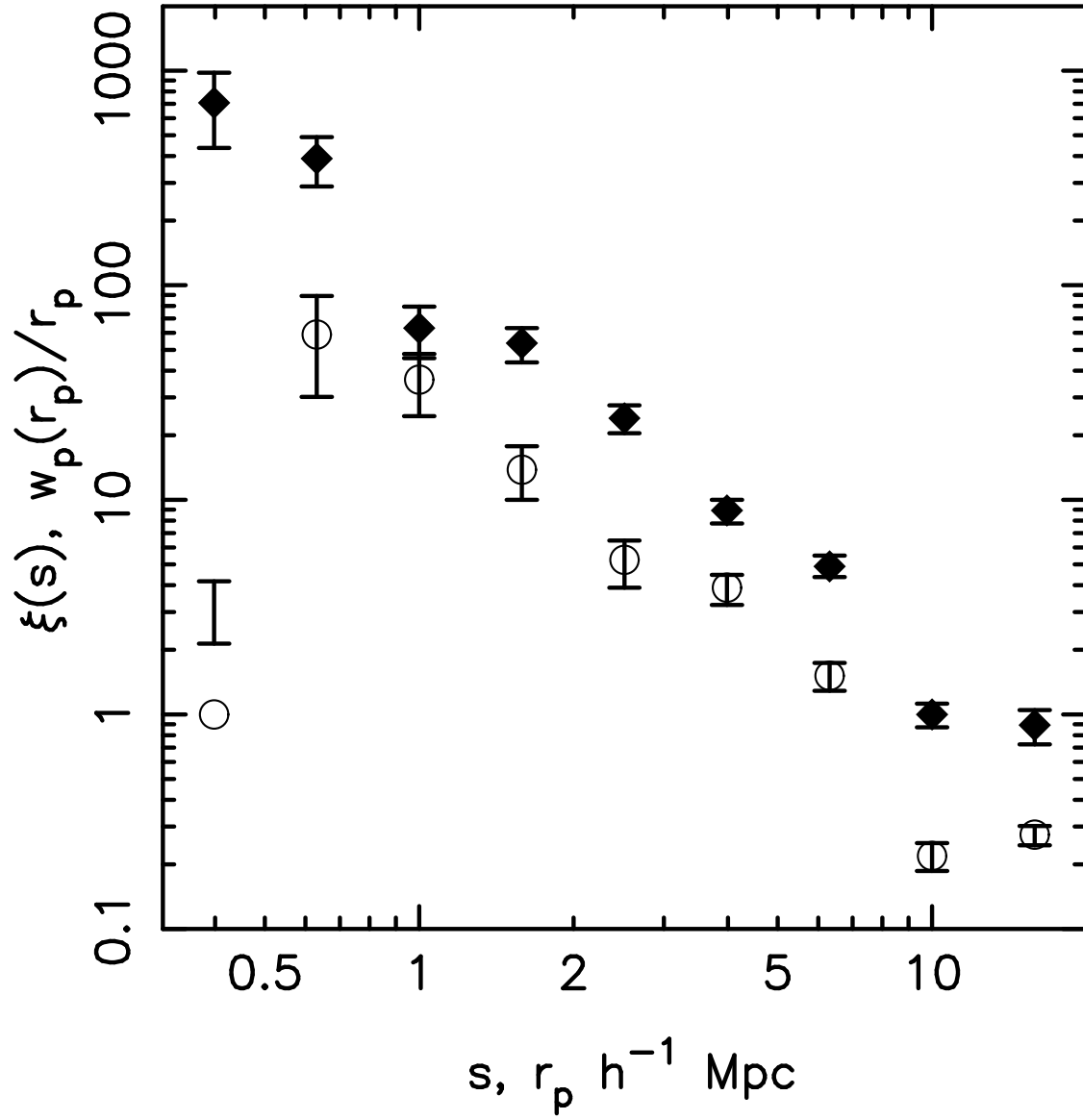


Fig. 7.—

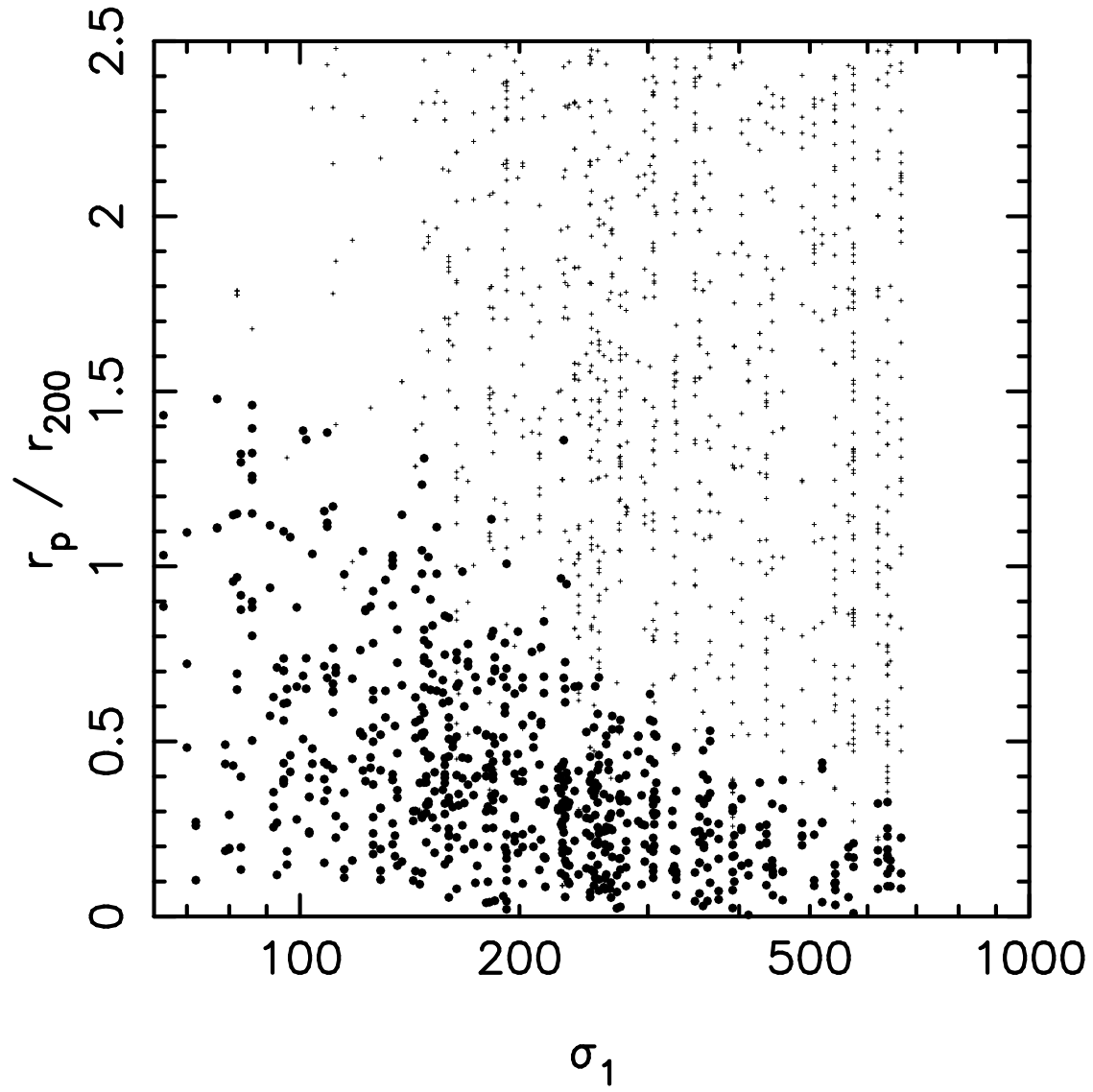


Fig. 8.—

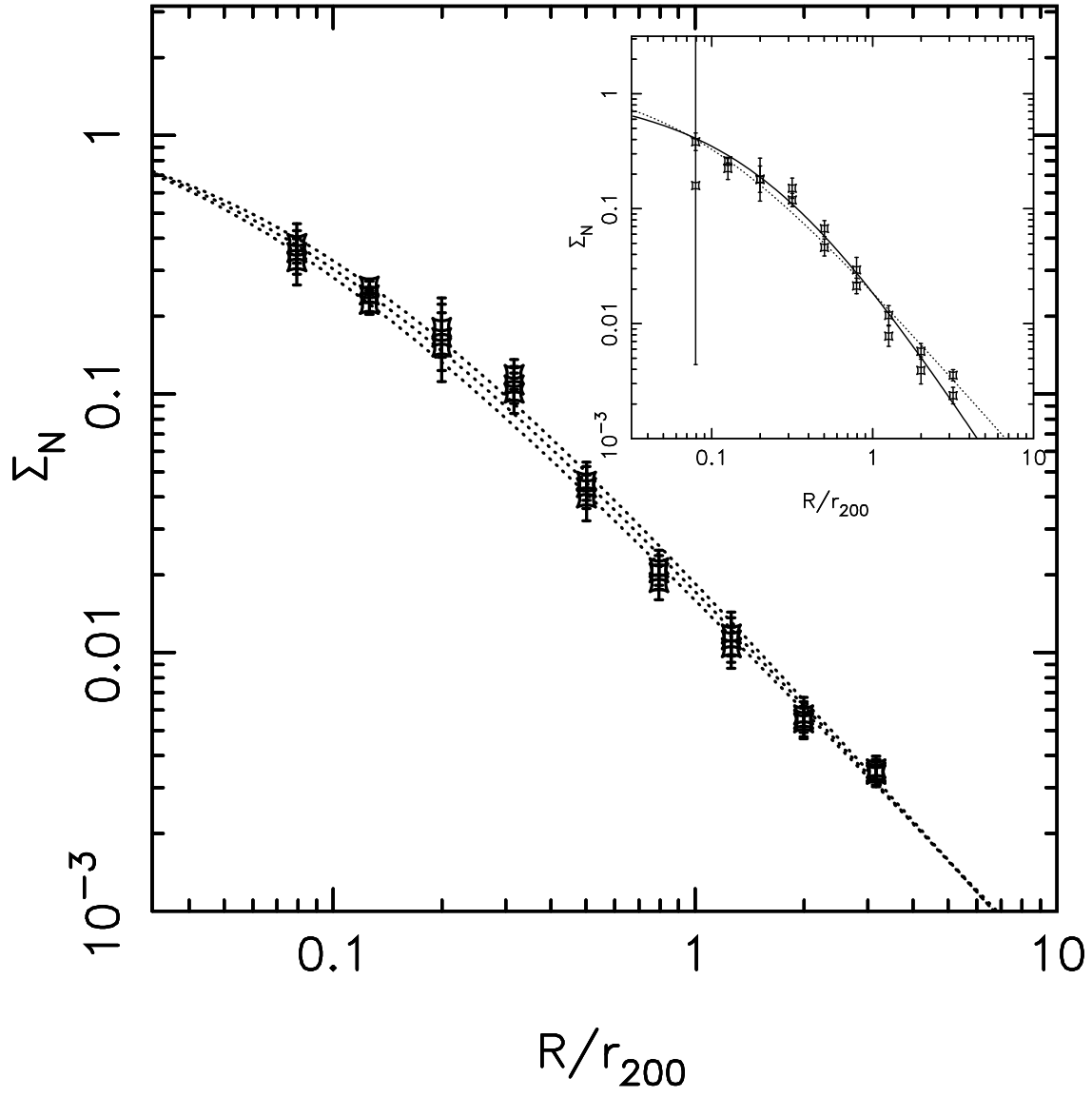


Fig. 9.—



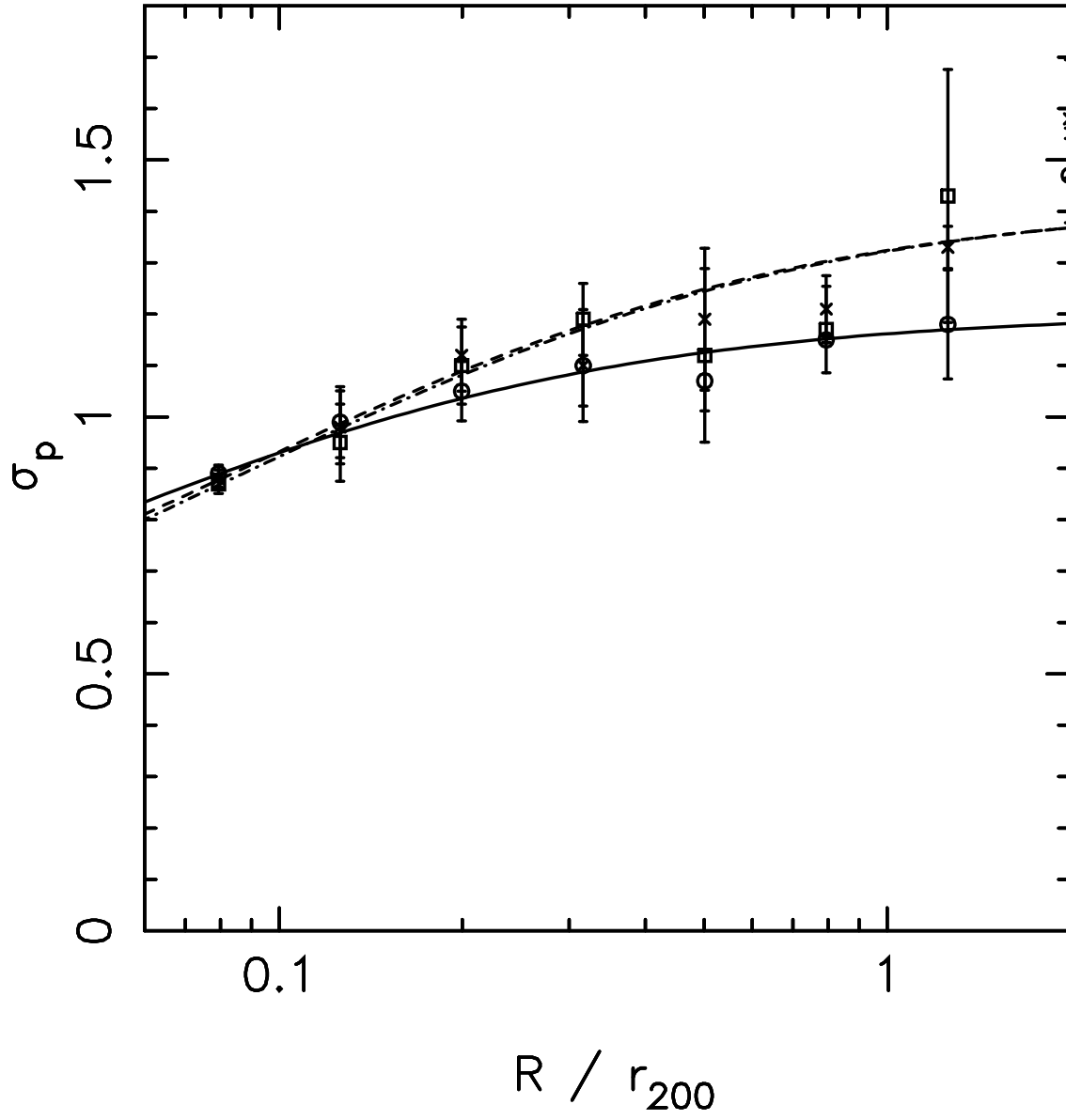


Fig. 10.—

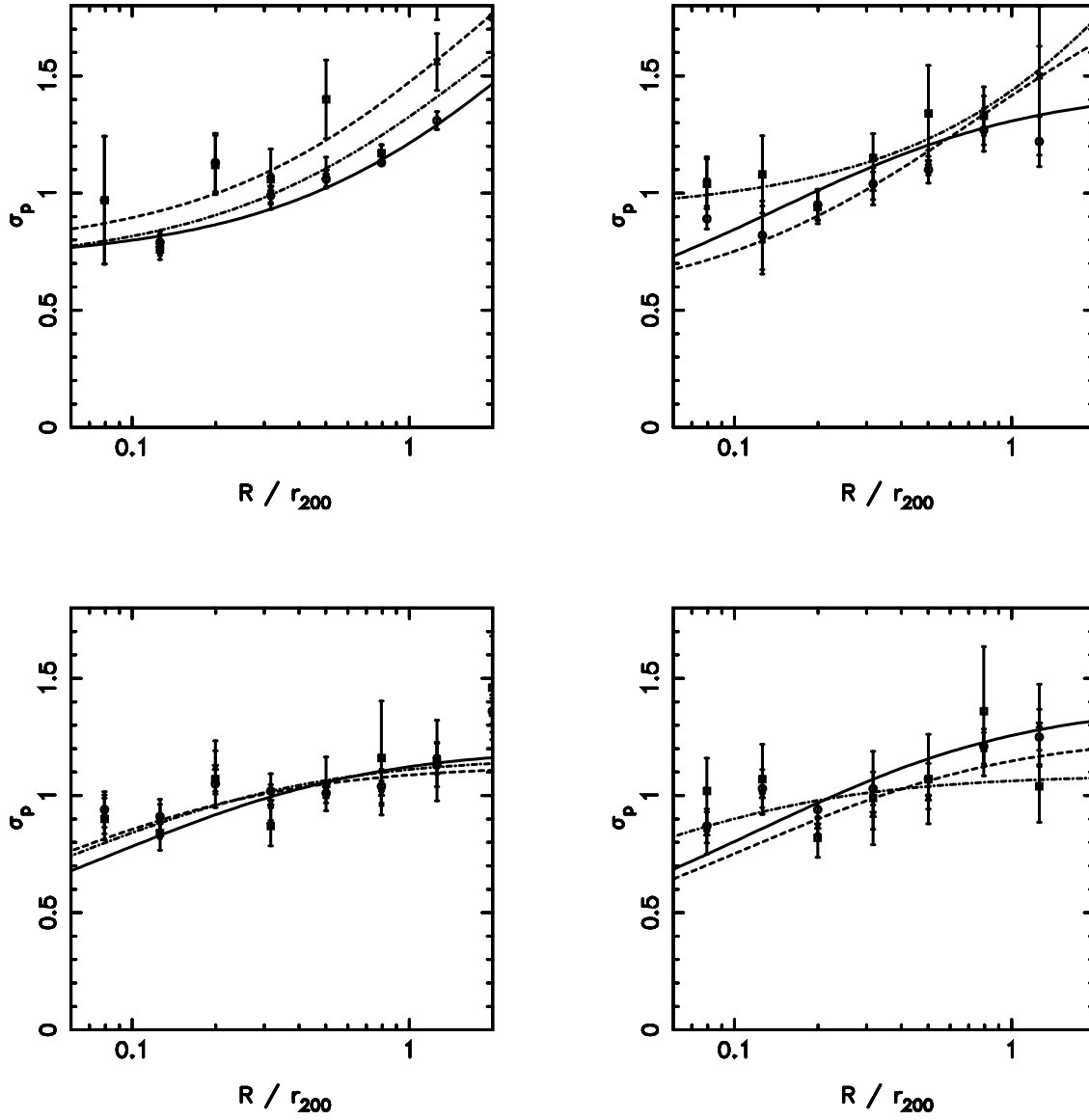


Fig. 11.—

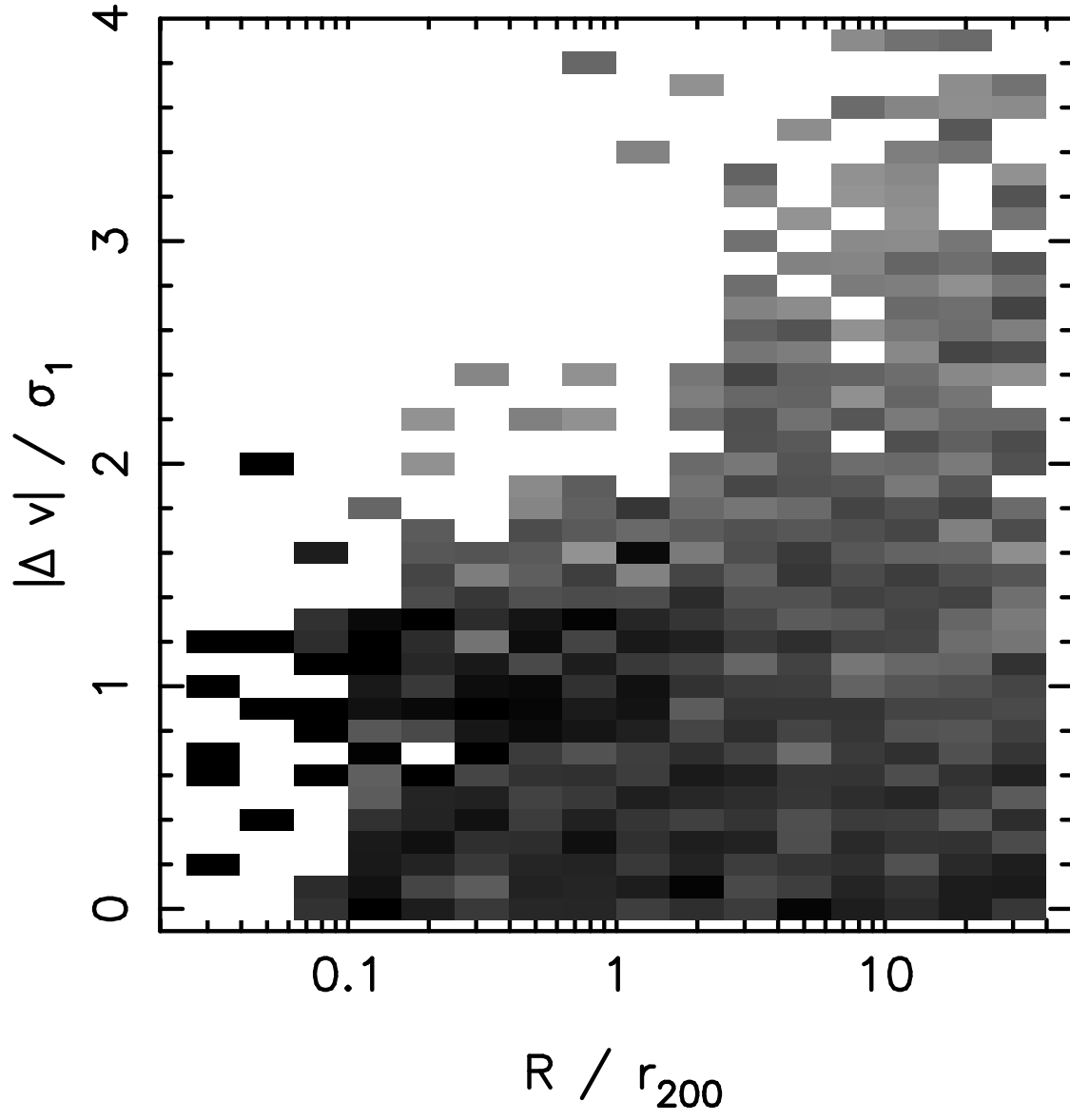


Fig. 12.—

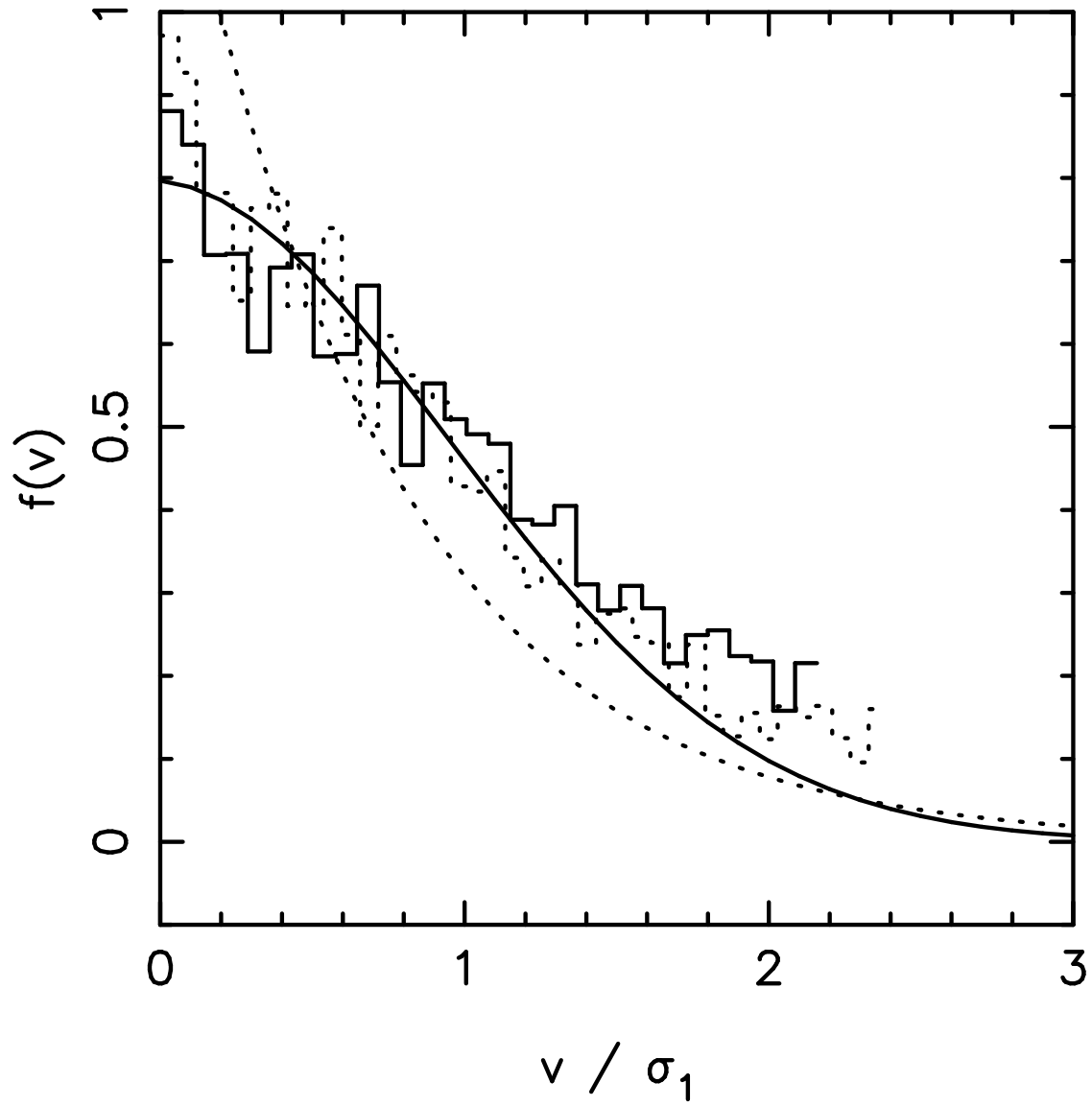


Fig. 13.—

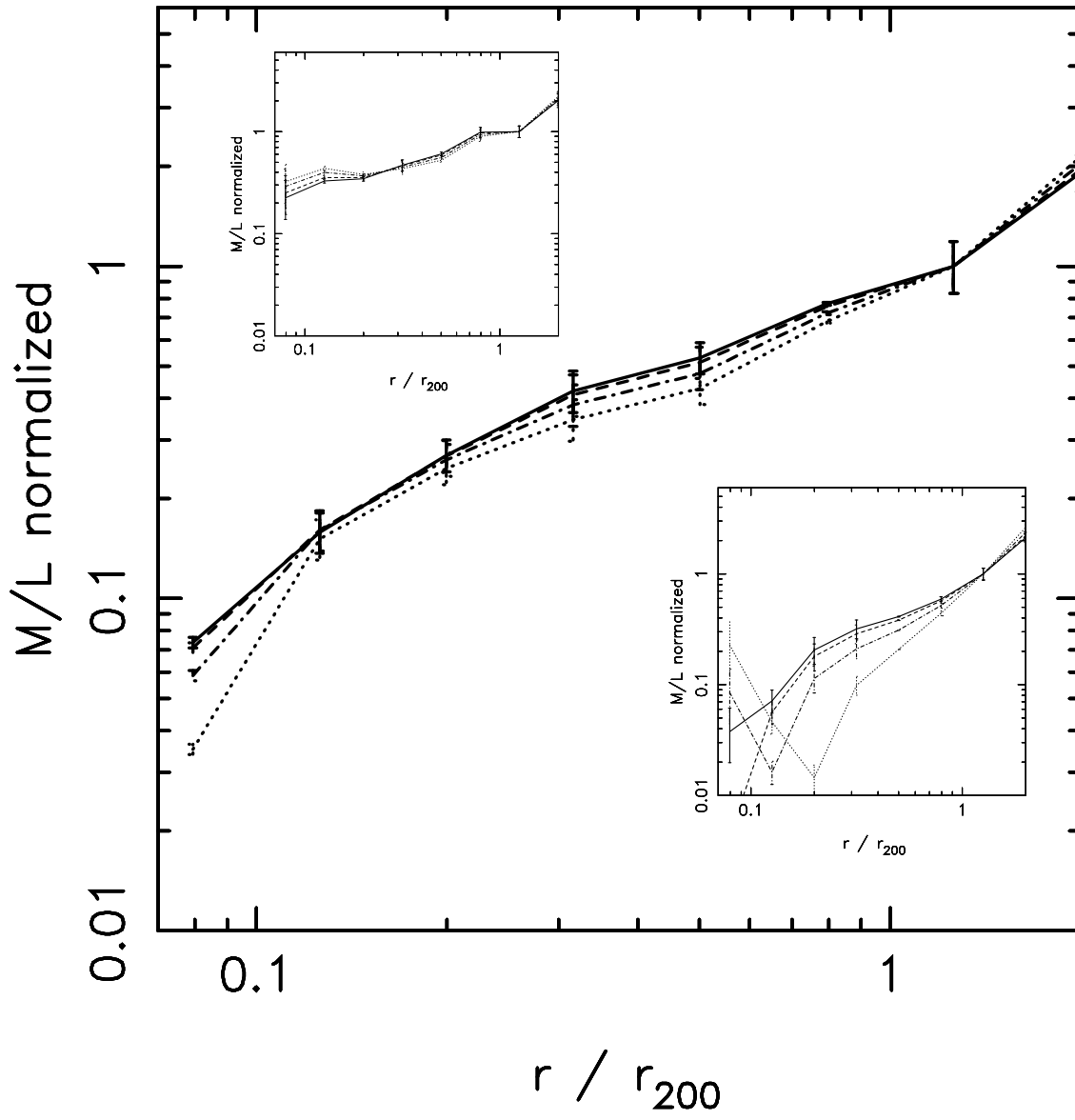


Fig. 14.—

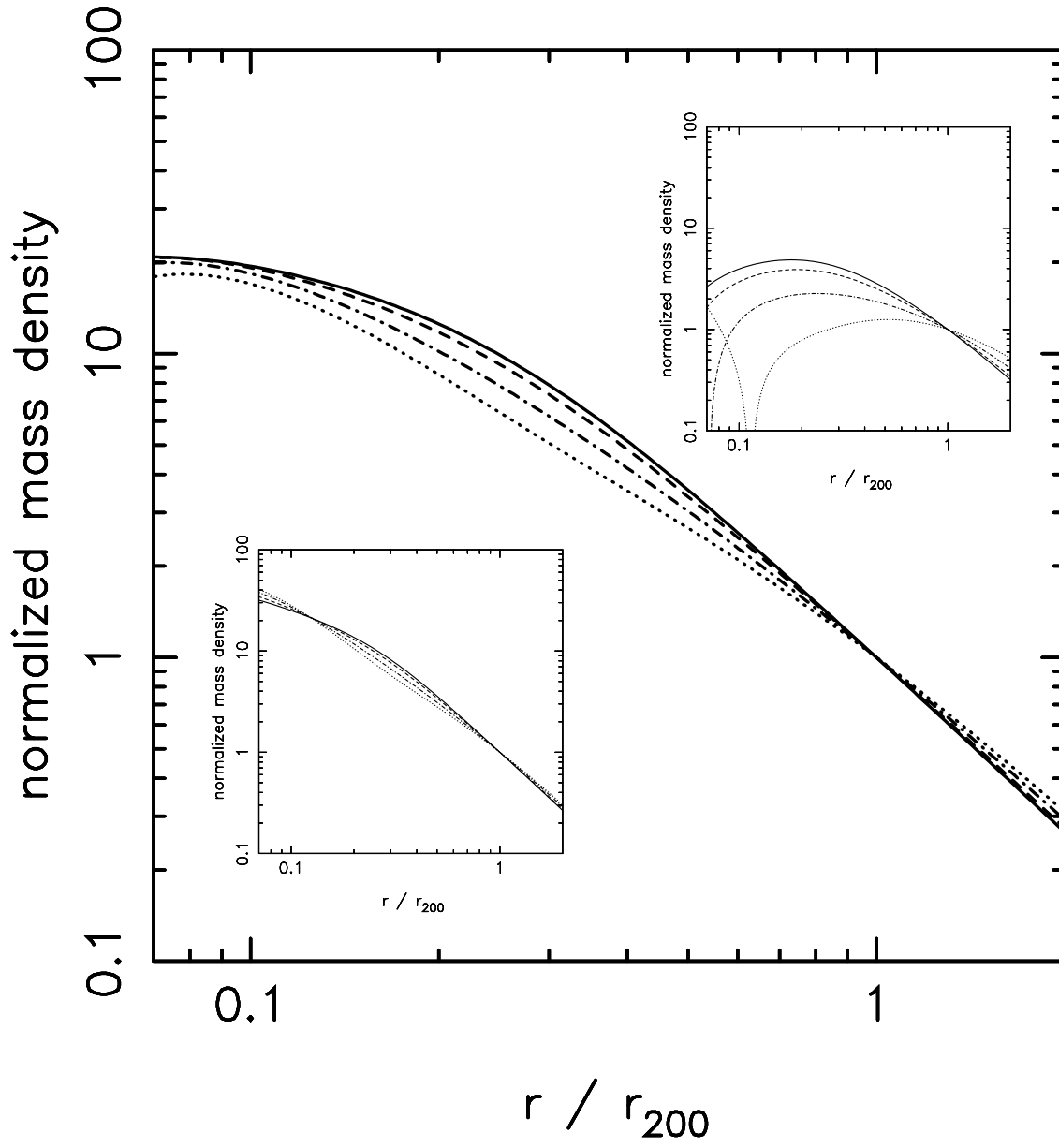


Fig. 15.—

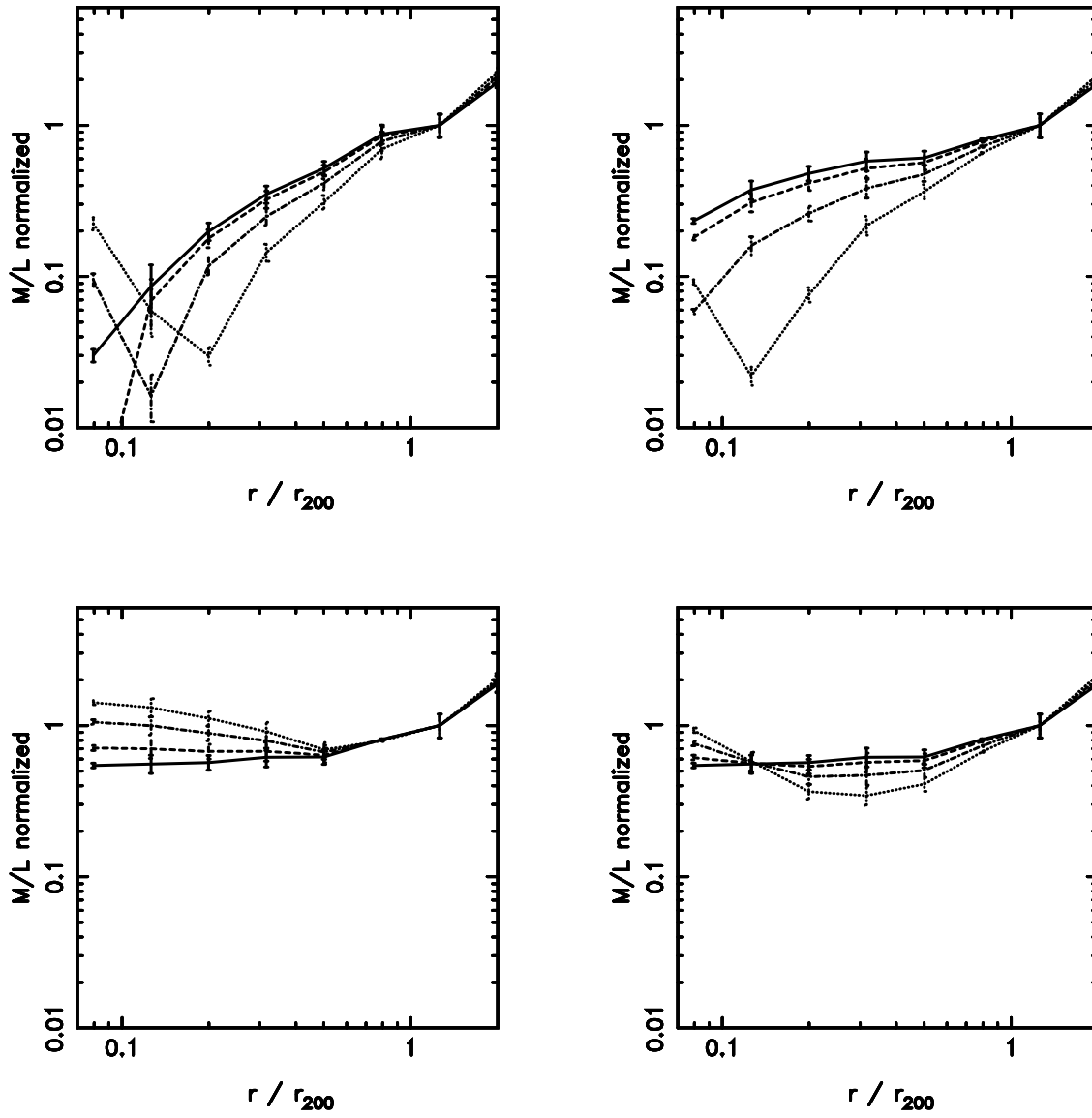


Fig. 16.—

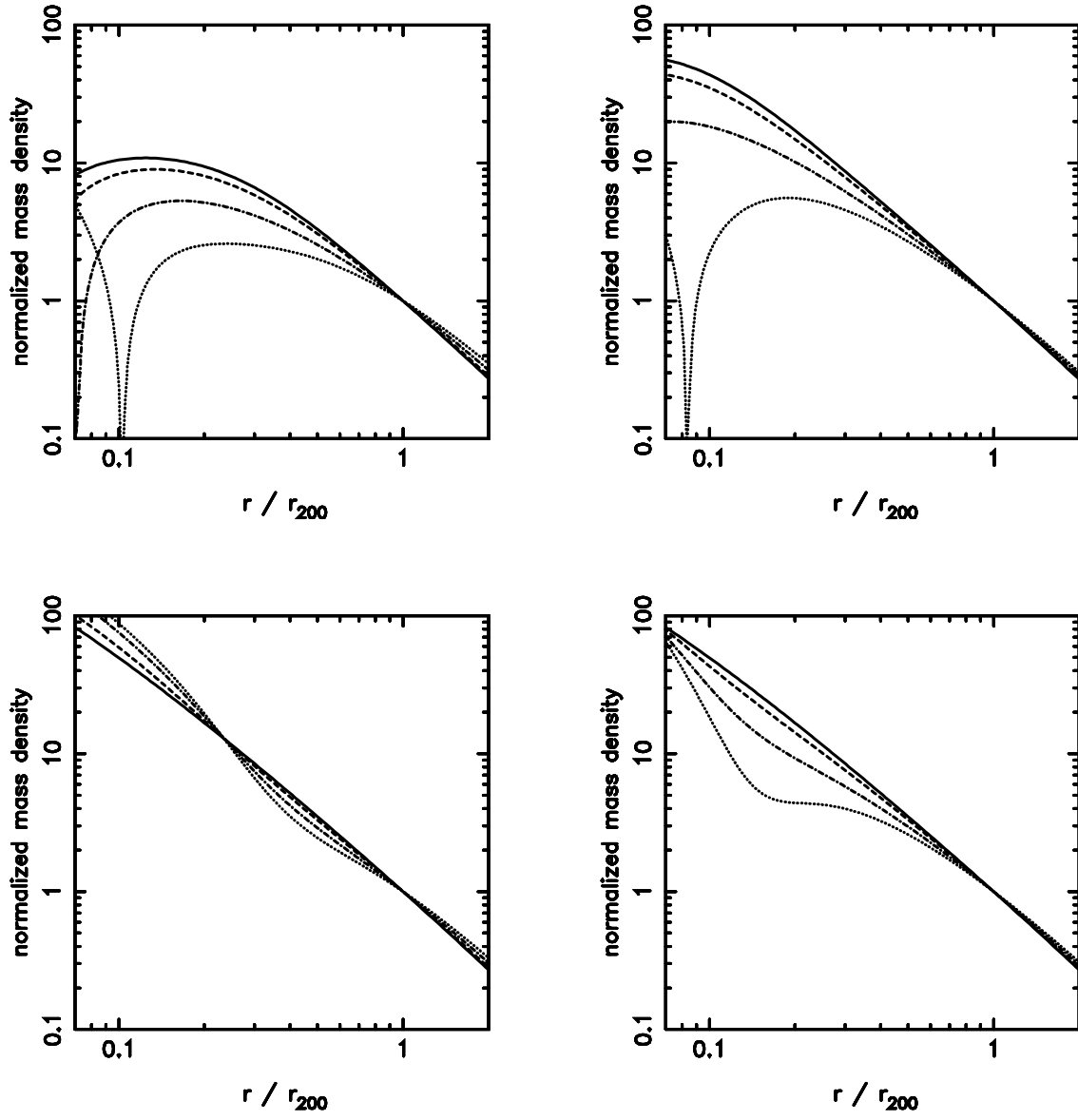


Fig. 17.—



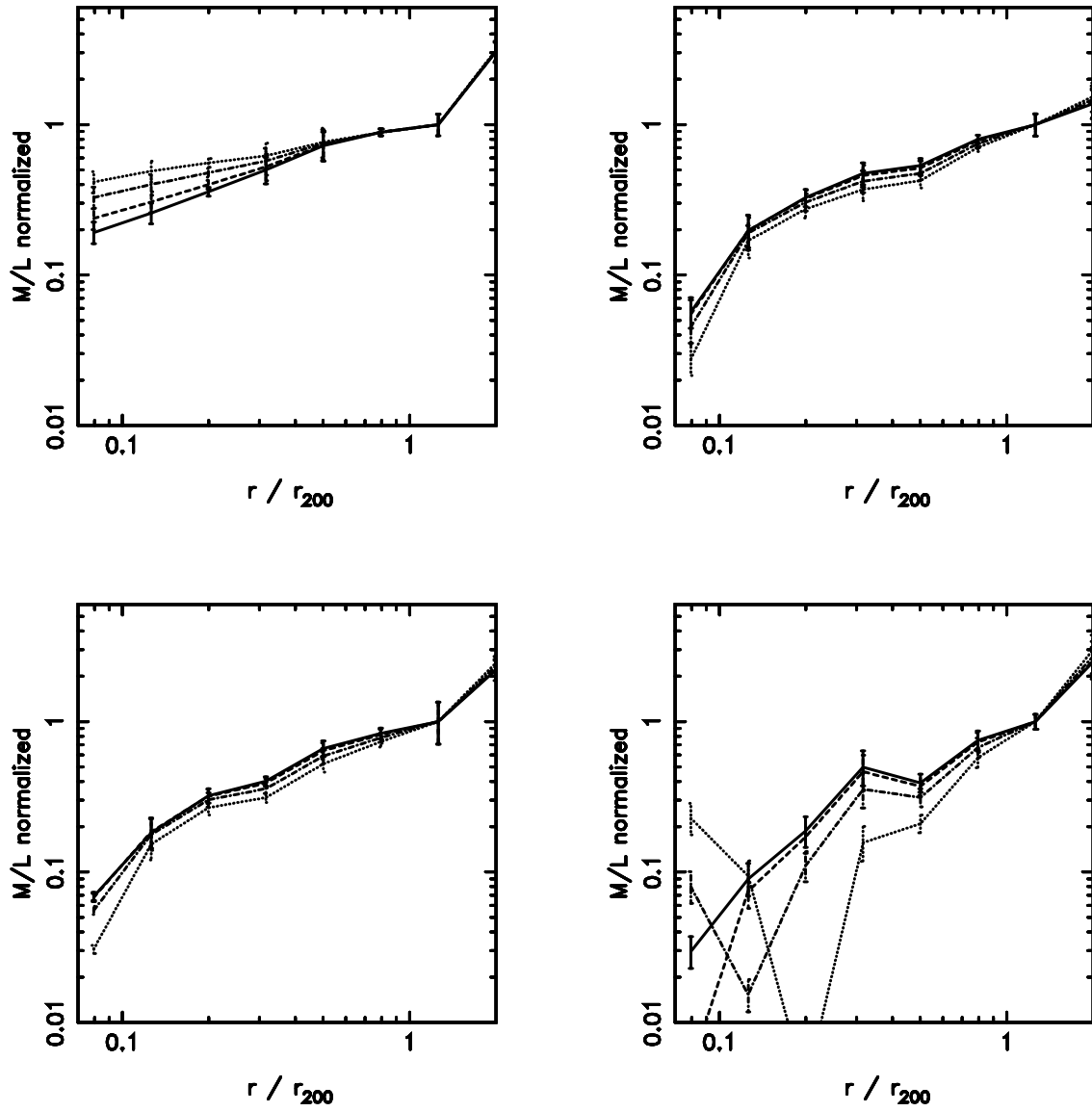


Fig. 18.—